



OPEN ACCESS

EDITED BY

Xiaojun Feng,
China University of Mining and
Technology, China

REVIEWED BY

Shengquan He,
University of Science and Technology
Beijing, China
Shouqing Lu,
Qingdao University of Technology, China

*CORRESPONDENCE

Junjun Feng,
✉ junjunf@ahut.edu.cn

RECEIVED 10 April 2025
ACCEPTED 05 May 2025
PUBLISHED 16 May 2025

CITATION

Feng J, Li S, Xu C, Peng J and Huang Q (2025)
Assessing the thermal cracking process of
coal in high-temperature environment: an
ultrasonic approach.
Front. Earth Sci. 13:1609410.
doi: 10.3389/feart.2025.1609410

COPYRIGHT

© 2025 Feng, Li, Xu, Peng and Huang. This is
an open-access article distributed under the
terms of the [Creative Commons Attribution
License \(CC BY\)](https://creativecommons.org/licenses/by/4.0/). The use, distribution or
reproduction in other forums is permitted,
provided the original author(s) and the
copyright owner(s) are credited and that the
original publication in this journal is cited, in
accordance with accepted academic practice.
No use, distribution or reproduction is
permitted which does not comply with
these terms.

Assessing the thermal cracking process of coal in high-temperature environment: an ultrasonic approach

Junjun Feng^{1,2*}, Shigeng Li², Chuanhua Xu¹, Jun Peng¹ and Qisong Huang¹

¹Sinosteel Maanshan General Institute of Mining Research Co., Ltd., Maanshan, China, ²Civil Engineering and Architecture, Anhui University of Technology, Maanshan, Anhui, China

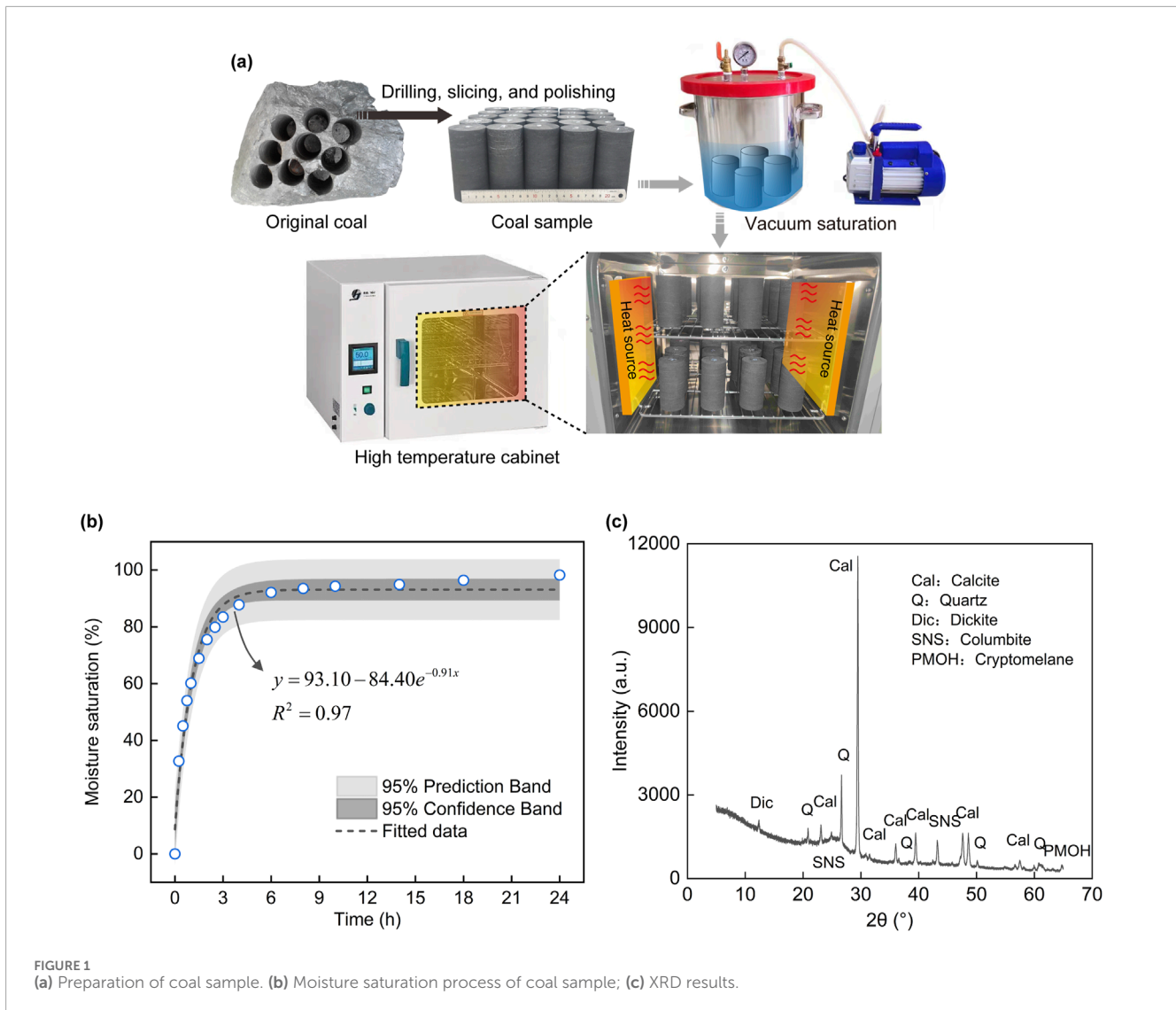
Thermal cracking of coal in high-temperature environments poses a significant challenge to the sustainability of deep coal mining. It increases the risk of coal and gas outbursts and spontaneous combustion and also contributes to groundwater pollution and greenhouse gas emissions, ultimately undermining the environmental sustainability of coal mining. This study investigates the coal thermal cracking in such environments and introduces an ultrasonic approach to evaluate the thermal cracking process. The results indicate a positive correlation between crack opening and cumulative moisture desorption, as well as between crack expansion rates and moisture desorption rates. In addition, the ultrasonic P-wave shows a robust response to both moisture desorption and thermal cracking, supported by nonlinear and linear models correlating wave velocity and attenuation coefficient, respectively. In addition, a theoretical model elucidates the driving forces, including surface tension and vapor pressure, that contribute significantly to thermal cracking at high temperatures. The ultrasonic method based on the theoretical model provides an innovative approach for assessing the coal thermal cracking process, contributing to improved environmental sustainability in deep coal mining.

KEYWORDS

deep coal mining, thermal cracking assessment, high-temperature environment, ultrasonic approach, moisture desorption

1 Introduction

As the global demand for mineral resources continues to grow, the coal mining industry is gradually shifting to deep resources. However, deep coal resources are often characterized by high temperatures due to the geothermal gradient, which poses great challenges to coal mining (Huang, et al., 2023). For example, the average temperature in Ordos Basin is about 32°C with a burial depth of 488.0–1,324.8 m (Li, et al., 2018); the temperature in the Black Warrior Basin reaches 50°C at a depth of approximately 2000 m (Pashin and McIntyre, 2003); and the temperature in the Bide-Santang Basin reaches 63.4°C at a depth of 1,500 m (Guo, et al., 2020). In such deep, high-temperature environments, the thermal cracking behavior of coal poses a significant impact on the efficiency and safety of coal mining, which refers to the phenomenon where cracks expand in coal due to thermal stress accumulation under high temperatures (Sun, et al., 2022). This phenomenon not only



weakens the mechanical properties of the coal, but also significantly changes its permeability, thereby affecting the transport of gas, air, and moisture within the deep coal seam.

Thermal cracking poses serious challenges to the environmental sustainability of deep coal mining. First, the cracks created by thermal cracking in high-temperature environments provide additional migration pathways for gas, leading to rapid desorption and release of gas, increasing the risk of coal and gas outburst disasters (Yang, et al., 2023). In addition, the cracks created by thermal cracking create diffusion pathways for oxygen, accelerating the oxidative spontaneous combustion process of coal, resulting in the waste of coal resources and the release of large amounts of greenhouse gases (Carras et al., 2009). Moreover, the thermal cracking of coal can also affect groundwater systems, as the expansion of cracks can facilitate the upward migration of groundwater containing heavy metals and other potential hazards, seriously degrading groundwater quality (Hamada et al., 2024). Therefore, in-depth research on the characteristics of coal thermal cracking under high-temperature conditions and its monitoring technologies is crucial not only for improving the safety of deep coal

mining but also for achieving the environmental sustainability of mining operations.

The main issue in the study of coal thermal cracking is the accurate detection of cracks. Current detection methods can be divided into two main categories: physical detection and acoustic detection. Physical detection methods leverage the irreversible nature of coal cracking, allowing for quantitative assessment of crack parameters by comparing results obtained before and after treatment. These methods include mercury intrusion porosimetry (MIP), scanning electron microscopy (SEM), nuclear magnetic resonance (NMR) (Li et al., 2019; Li et al., 2024), and X-ray computed tomography (CT) (Salmachi et al., 2024). For example, the SEM testing revealed that the number and length of cracks increased with temperature (Yang et al., 2019). The combined MIP and SEM testing indicated that microwave heating facilitated the opening, enlargement, and interconnection of pores, while the non-uniform thermal stresses induced by microwave heating contributed to the enlargement of existing cracks and the formation of new ones (Lin et al., 2021). The CT testing showed that heat treatment significantly influenced the crack morphology of coal, with both crack aperture and permeability increasing at a high

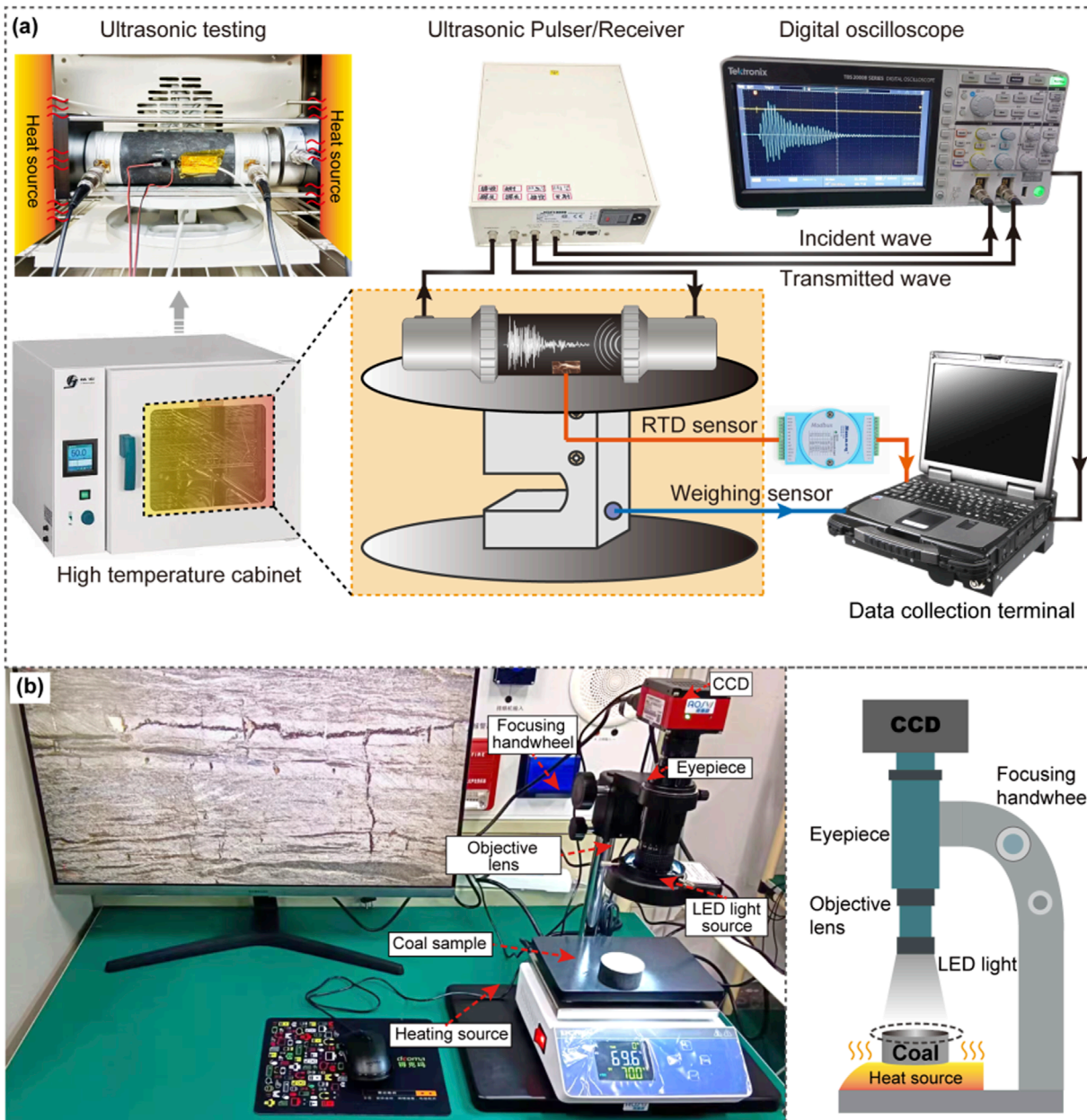
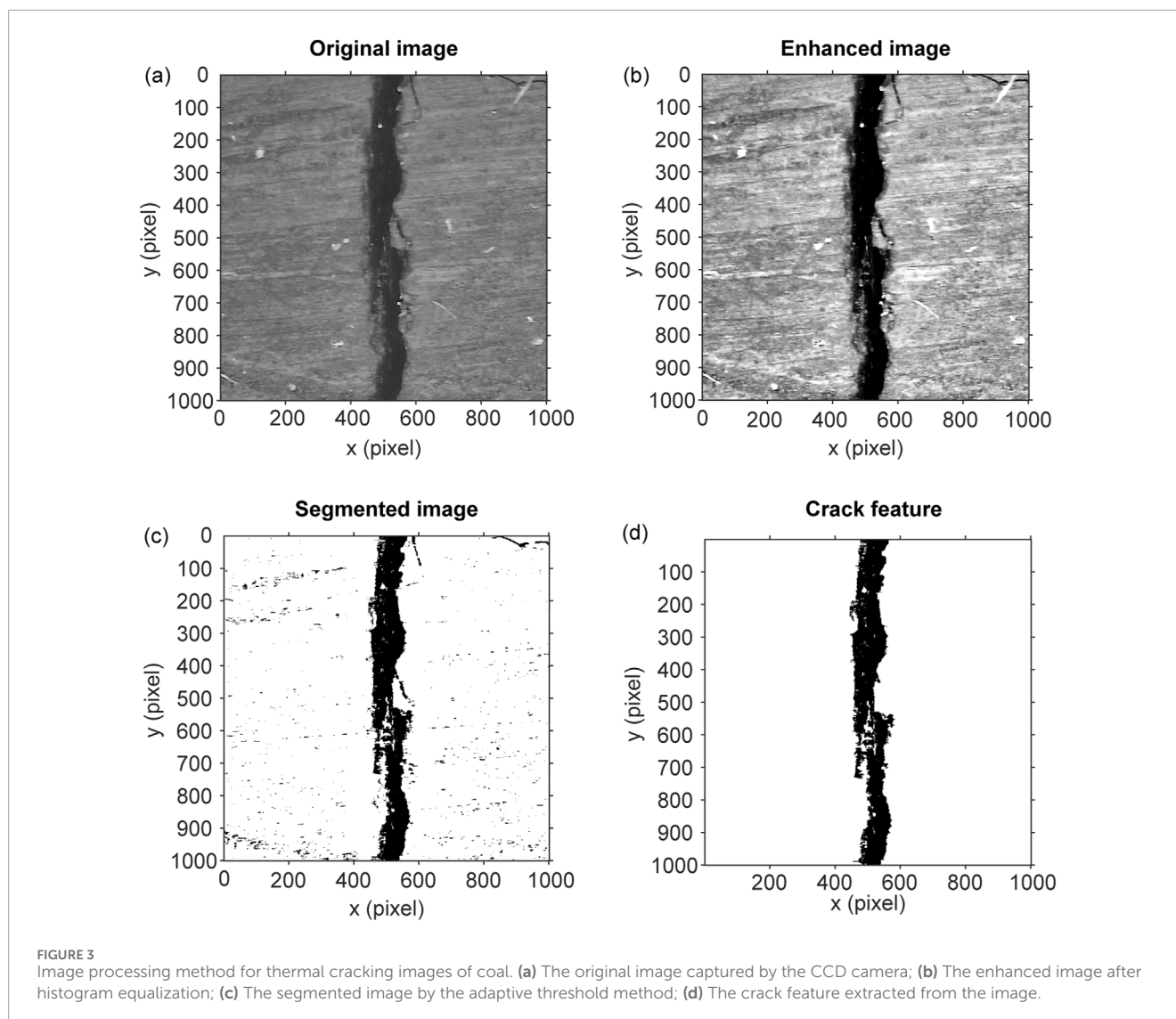


FIGURE 2 Experimental system for thermal cracking of coal under the high-temperature environment. (a) Ultrasonic testing system; (b) Digital imaging system.

temperature (Liu et al., 2020; Salmachi et al., 2024). The NMR testing demonstrated that cyclic thermal treatment can effectively promote the formation and expansion of seepage pores in the coal (Jiang et al., 2021). However, these physical detection methods rely heavily on complex instrumentation, making them difficult to implement directly in *in-situ* coal seams.

The ultrasonic approach, as a typical acoustic detection method, has been extensively used for crack detection due to its good adaptability to *in situ* coal seams (Cai et al., 2014). The ultrasonic approach relies on the acoustic wave propagation characteristics that are strongly associated with the pores and fractures in coal seams, including wave velocity and wave attenuation (Zhang et al., 2021). For instance, a significant relationship exists between the porosity

and the velocity of ultrasonic P-waves (Kahraman and Yeken, 2008). Furthermore, the morphology of pores influences the ultrasonic P-wave velocity; specifically, the presence of micropores and interlayer porosity results in a reduction of ultrasonic wave velocity (Soete, 2015). Additionally, a correlation has been established between the fracture parameters of rocks and both P-wave and S-wave velocities, as well as the ratio of V_p/V_s . Notably, both P-wave and S-wave velocities increase with an increase in fracture parameters, while the V_p/V_s ratio rises as the fracture parameter decreases (Leucci and De Giorgi, 2006). The aperture of fractures also significantly impacts wave velocity (Wei et al., 2013). In contrast to rocks, coal features a more intricate network of pore and fissure structures, often containing significant amounts of fluids such as



water and gas. Some researchers have investigated the effects of water and gas adsorption on ultrasonic wave velocity, concluding that adsorption-induced matrix expansion reduces fracture openings, thereby enhancing sensitivity to fluid adsorption (Lv et al., 2022).

Thermal cracking is not the only change that occurs in coals at high temperatures; it is often accompanied by moisture desorption, which has been observed in both laboratory tests and field studies (Akbarzadeh and Chalaturnyk, 2014; Teng et al., 2016; Yu et al., 2012). However, the relationship between moisture desorption and thermal cracking in water-bearing coal is not well understood, and an effective method for evaluating the thermal cracking of coal is still needed. This study aims to investigate the thermal cracking of water-bearing coal in a high-temperature environment, focusing on the correlation between thermal cracking and moisture desorption. Furthermore, the influence mechanism of moisture desorption on the thermal cracking of coal has been fully discussed. Finally, this research proposes an ultrasonic approach for evaluating thermal cracking in coal. The results of this study have significant implications for evaluating thermal cracking in coal seams and improving environmental sustainability in deep coal mining.

2 Materials and methods

2.1 Sample preparation

The coal samples utilized in this study were sourced from the Ordos mining area in Inner Mongolia, China. To minimize variability in physical properties, all samples were collected from the same coal seam, ensuring that the surfaces of the selected raw coal lumps were dense and devoid of cracks. The raw coal was subsequently drilled, cut, and polished into cylindrical samples with a diameter of 50 mm and a length of 100 mm, as illustrated in Figure 1a. Industrial analytical tests revealed that the samples contained less than 37% volatile content, classifying them as bituminous coals. To ensure uniform saturation, a vacuum saturation device was employed to saturate the specimens, followed by full saturation with water after degassing. Throughout the water saturation process, the specimens were weighed at regular intervals. They were classified as saturated once the mass variation was less than 0.1% within a 1-h timeframe. The mass change curve during this saturation process is depicted in

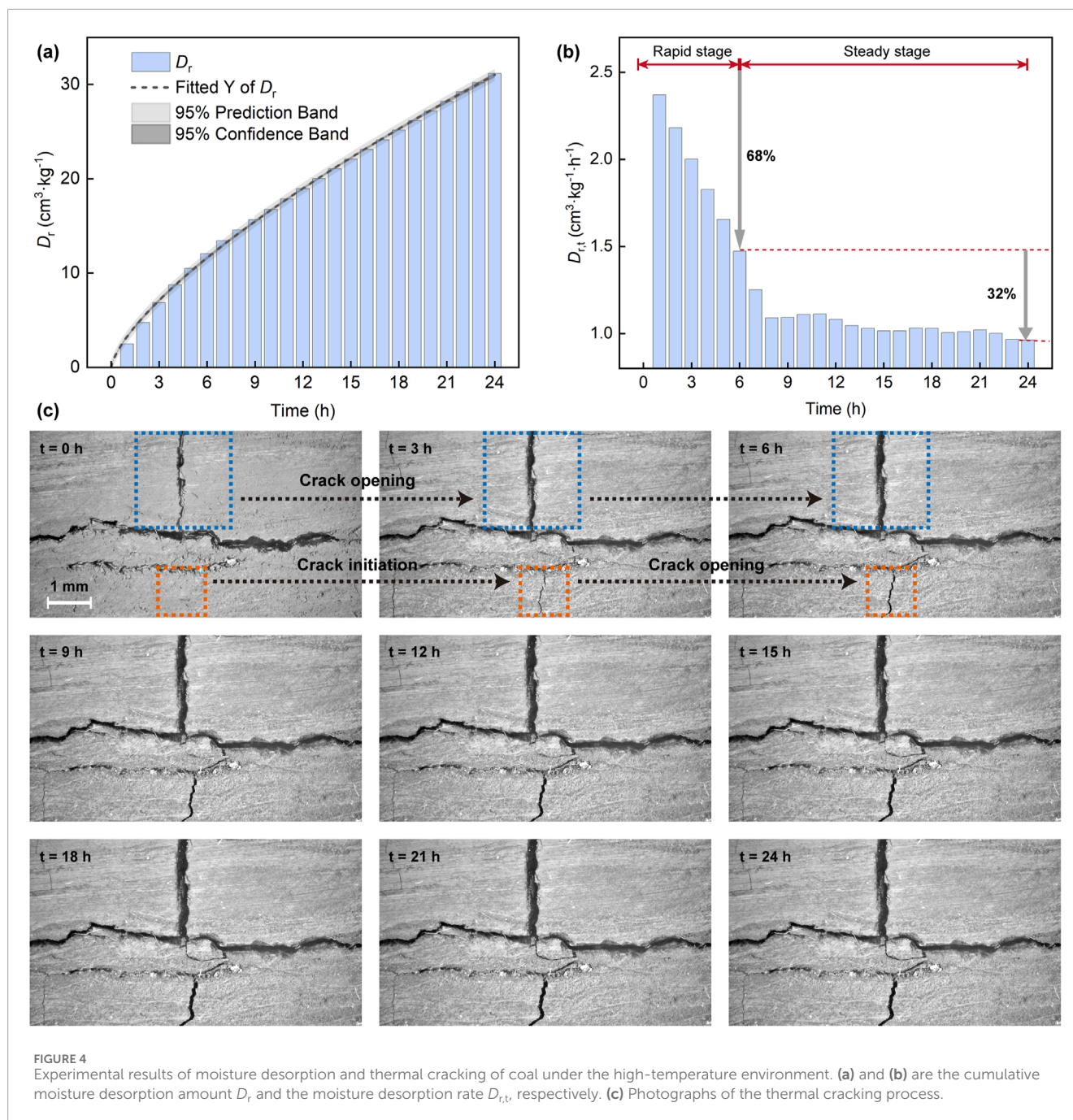


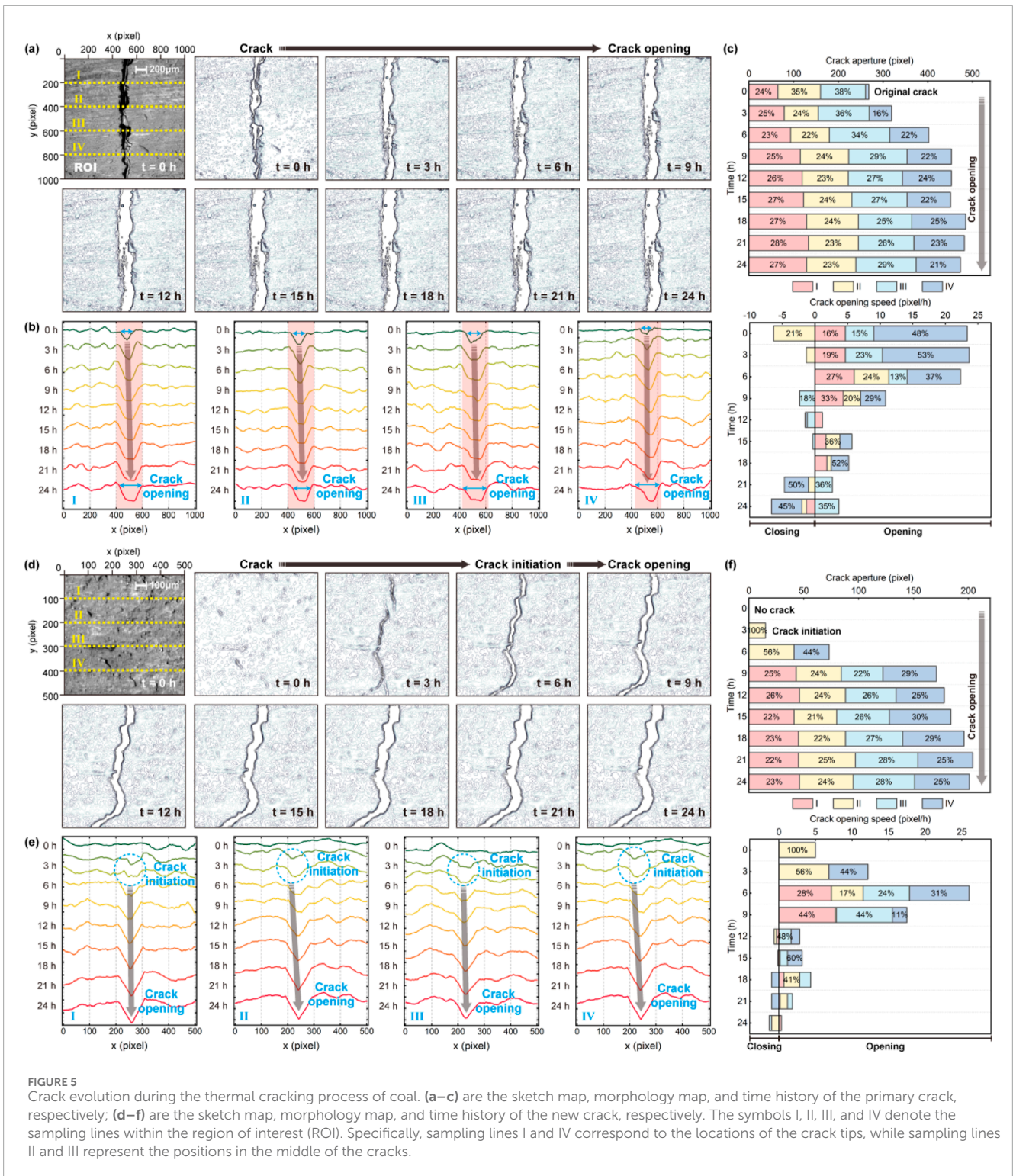
FIGURE 4 Experimental results of moisture desorption and thermal cracking of coal under the high-temperature environment. (a) and (b) are the cumulative moisture desorption amount D_r , and the moisture desorption rate $D_{r,t}$, respectively. (c) Photographs of the thermal cracking process.

Figure 1b, showing that the mass of the samples stabilized after 9 h, indicating satisfactory saturation. Additionally, the results of X-ray diffraction (XRD) analysis of the samples, presented in Figure 1c, revealed the primary mineral components as calcite, quartz, and diorite.

2.2 Experimental system

The experimental system for the thermal cracking and ultrasonic testing of water-bearing coal under high-temperature conditions is illustrated in Figure 2a. This system comprises a high-temperature cabinet, a weighing sensor, an ultrasonic pulse generator/receiver,

a digital oscilloscope, and an RTD temperature sensor. The high-temperature cabinet provides a stable thermal environment for the experiment. The RTD sensor monitors temperature fluctuations in the cabinet. The weighing sensor captures real-time variations in the sample's mass in the high-temperature environment, allowing for the measurement of moisture desorption of the sample. In this study, we utilized an ultrasonic pulse generator (model DPR300), which features a negative-tip pulse type, a set frequency of 35 MHz, a pulse width of 50 ns, a transmitting voltage of 475 V, a repetition frequency of 100 Hz, and a gain of 42 dB. A contact probe with a diameter of 50 mm (model HS-DP100K) was employed, along with a high-temperature coupler as the coupling medium. Data acquisition was performed using an ultrasonic oscilloscope (model TBS2000B),



which had a sampling rate of 100 MHz and a low-pass filter set to 10 MHz. Each data point was collected 100 times and averaged to enhance the signal-to-noise ratio, with the attenuation coefficient of the probe set at 10x.

This study selects 50°C as the experimental temperature based on several considerations. Firstly, in China, most coalbed methane (CBM) reservoirs are located at depths of less than 2000 m,

where the maximum rock temperature is approximately 50°C. In addition, 50°C serves as the equilibrium point for the thermal expansion of the coal and the effects of stress, which significantly influences the expansion of internal fractures and the thermal cracking behavior of the coal (Akbarzadeh and Chalaturnyk, 2014). Secondly, too high-temperature environment can cause significant internal changes in coal, which in turn affect the stability

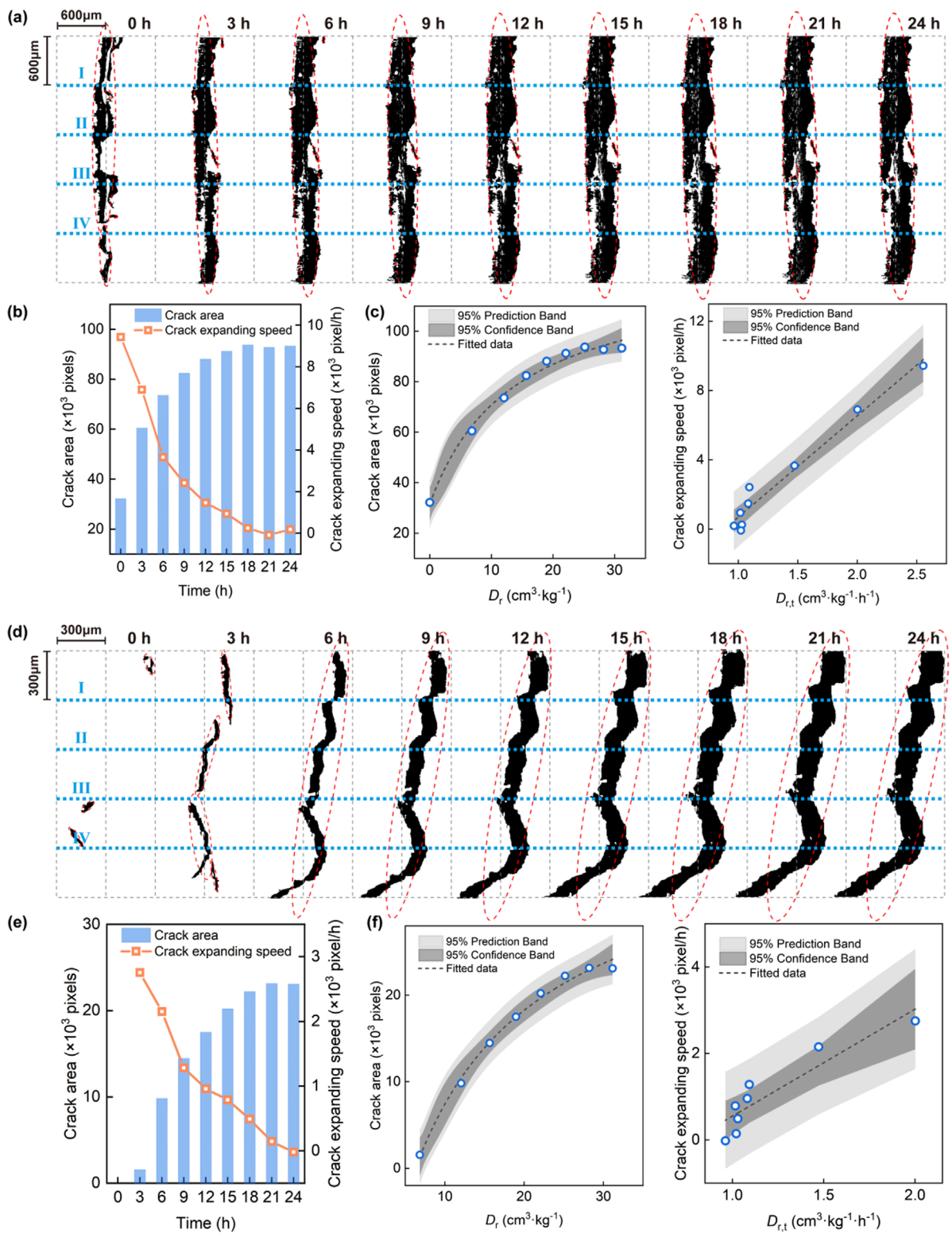


FIGURE 6 Relationship between thermal cracking and moisture desorption in water-bearing coal. (a, d) is the binary images of primary and newly formed cracks, respectively; (b, e) is the time history of crack feature parameters, including crack area and crack area change rate, for primary and new cracks, respectively; (c, f) are the fitting results of the thermal cracking parameters with the moisture desorption parameters.

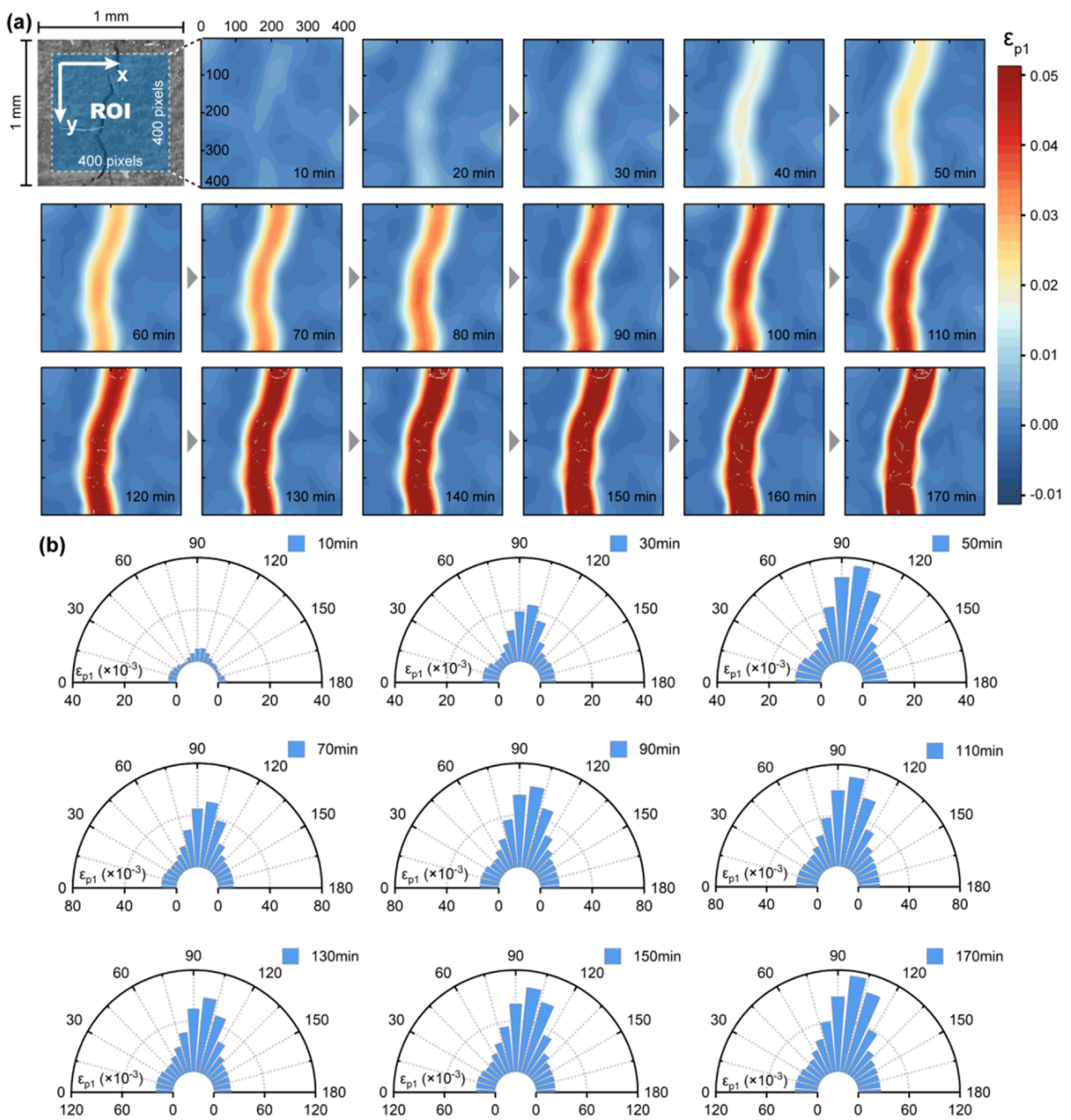
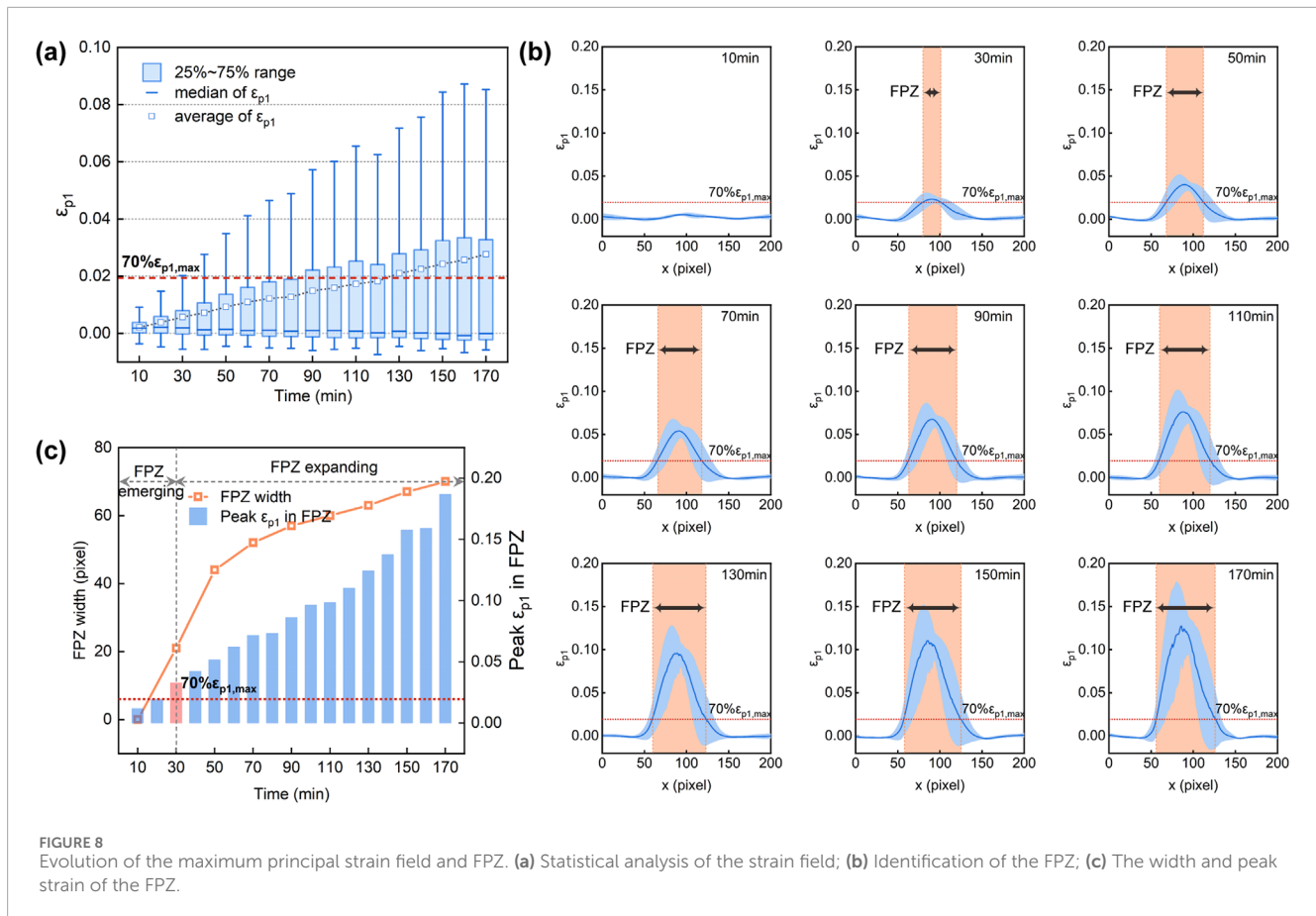


FIGURE 7 The maximum principal strain field evolution during the thermal cracking of water-bearing coal. (a) Strain field distribution; (b) Strain field orientation.

of experimental results. Some researchers have investigated the relationship between the porosity of coal samples and temperature through mercury intrusion experiments and found that the porosity increases significantly (Xiao et al., 2024). Thus, selecting 50°C as the temperature can help avoid drastic changes in coal porosity due to excessively high temperatures, thus ensuring the stability and reliability of the experiments.

The thermal cracking behavior of coal was recorded using a digital imaging system as shown in Figure 2b. This system consists of a CCD camera, an eyepiece, an objective lens, LED lighting, and

a heating base. To analyze the cracking behavior of coal using the Digital Image Correlation (DIC) method as described in our paper, it is essential to create a speckle pattern on the coal surface. The procedure for generating this speckle pattern involves first applying a layer of black matte paint as a primer to the coal surface, followed by the application of white matte paint. The experimental procedure is as follows: first, the heating base is set to the desired temperature, and the specimen with the speckle pattern is positioned on the heating base. The main objective lens is then adjusted to select the appropriate magnification to ensure that the speckle pattern is



within the optimum range for clarity. Finally, the Region of Interest (ROI) is defined within the captured images and the crack behavior is identified and analyzed.

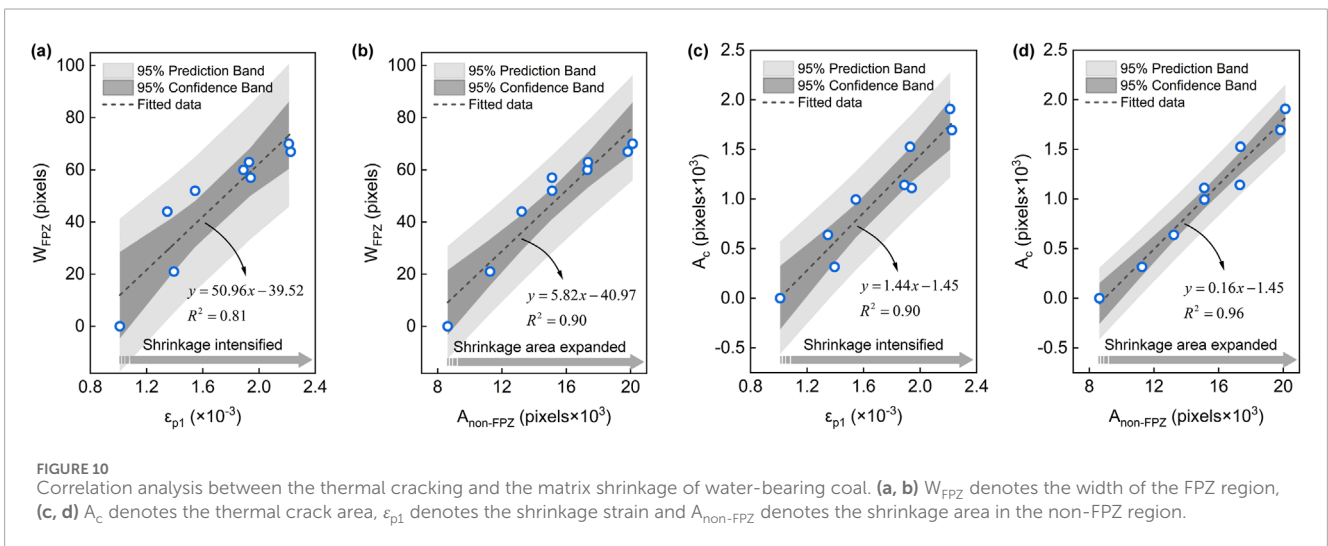
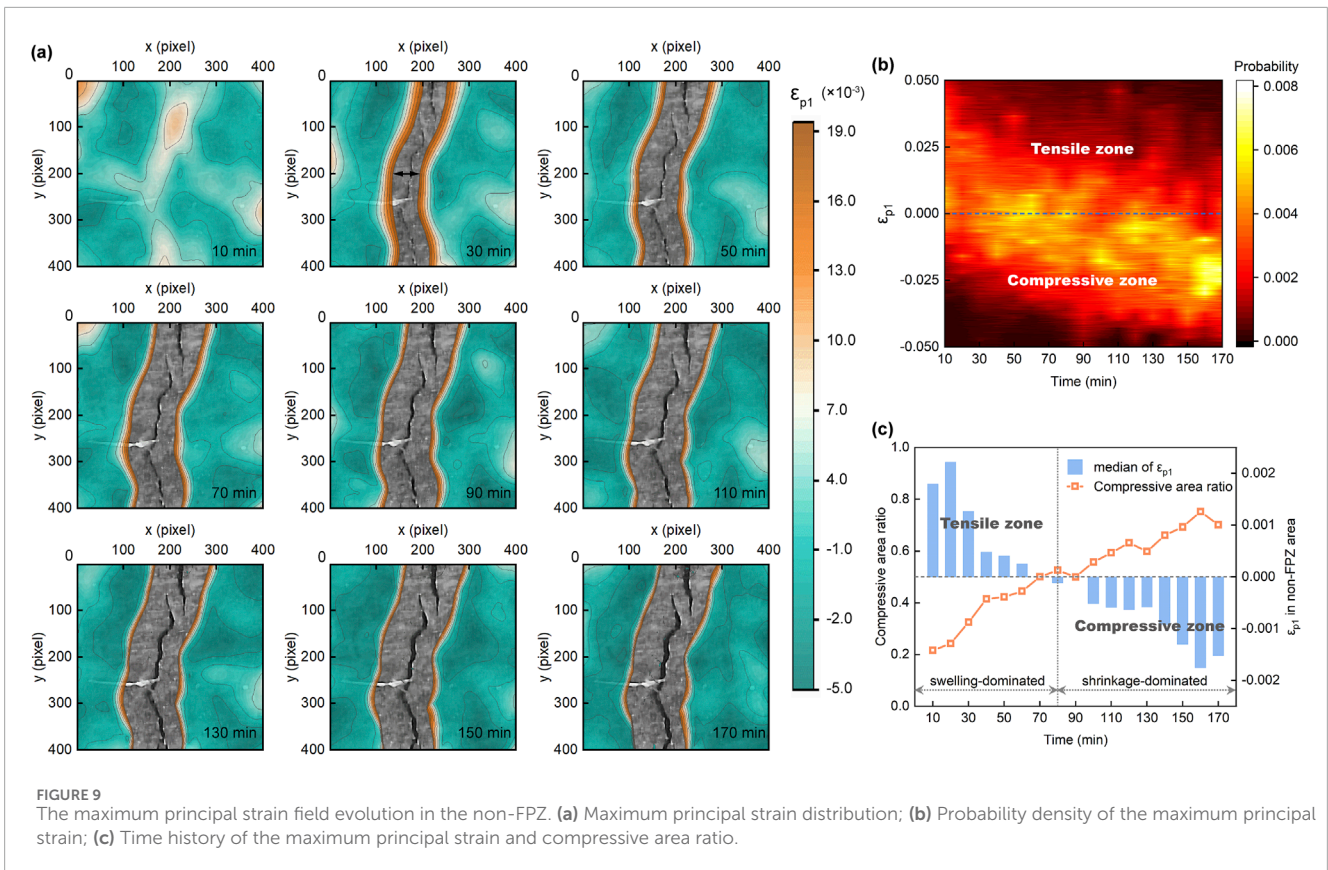
The original images of coal thermal cracking captured by the CCD camera are often of poor quality. Therefore, it is essential to improve the accuracy and reliability of crack feature identification, which requires the application of the image processing method to provide a reliable database for subsequent thermal crack analysis. In this study, several image processing techniques are applied, mainly histogram equalization, threshold segmentation, and morphological methods. As shown in Figure 3a, the inherent dark coloration of the coal sample results in insufficient contrast in the original image. To improve the image quality, we first apply histogram equalization for contrast enhancement by restricting the gray level distribution to the interval [56, 158]. The processed results are shown in Figure 3b. In addition, this study implements an adaptive threshold segmentation method, setting the sensitivity parameter to 0.18, which effectively separates the crack region from the background, as shown in Figure 3c. However, the segmentation results still include some interference regions. Analysis shows that these interference regions are significantly different from the actual cracks in terms of pixel area, statistical distance, and morphological features. Therefore, we apply the binary image opening operation with an area threshold of 3,500 pixels to eliminate these interference regions, resulting in the accurate crack region shown in Figure 3d.

In addition, the strain field and fracture propagation zone (FPZ) during the thermal cracking of coal were analyzed by the Digital Image Correlation (DIC) method. According to the principles of the DIC method, the most critical parameters of the DIC algorithm are the subset size and the subset space. A smaller subset size results in higher resolution, but may also result in an increased number of noisy points in the displacement and strain fields. In our previous study (Feng, et al., 2024), we performed a parametric analysis to determine the optimal subset size, which showed that a subset size of 40 pixels provided the best resolution for the DIC method. Therefore, the subset size was set to 40 pixels and the subset space was set to one pixel to achieve the highest precision in the calculation results.

3 Results

3.1 Moisture desorption and thermal cracking process of coal in the high-temperature environment

The processes of moisture desorption and thermal cracking process occur simultaneously in water-containing coals under high-temperature conditions. The original data of the thermal cracking process is available in the Supplementary Video 1. Moisture content and moisture desorption rate are two different concepts. Moisture content refers to the ratio of the mass of



water contained in the coal to the mass of the dry coal sample, reflecting the amount of moisture retained by the coal. In contrast, the moisture desorption rate indicates the amount of moisture released from the coal under specific conditions, focusing on the desorption characteristics of the coal and involving the process of moisture migration from the coal sample to the external environment. According to these definitions, it is clear that the moisture desorption rate more directly reflects the ability of moisture within the coal to migrate and be released under specific

environmental conditions. This property is critical for studying the dynamic changes in moisture during processes such as drying and weathering. In comparison, moisture content serves as a static indicator, while moisture desorption rate accounts for the dynamic effects of high-temperature environmental factors on the moisture state. Therefore, the moisture desorption rate is more suitable for describing this process. We define the cumulative moisture desorption amount and moisture desorption rate as metrics to characterize the extent of moisture desorption and the speed of

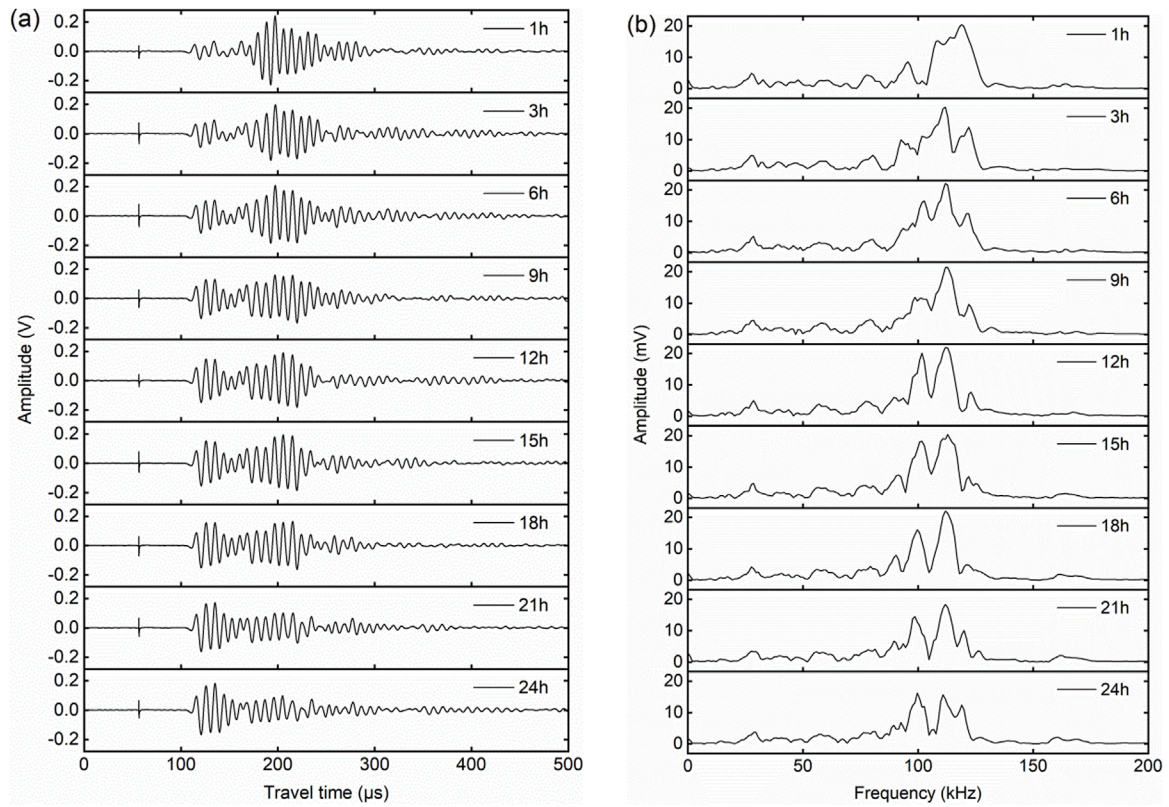


FIGURE 11 Ultrasonic results during thermal cracking of water-bearing coal. (a) Time domain waveforms; (b) Frequency domain spectra.

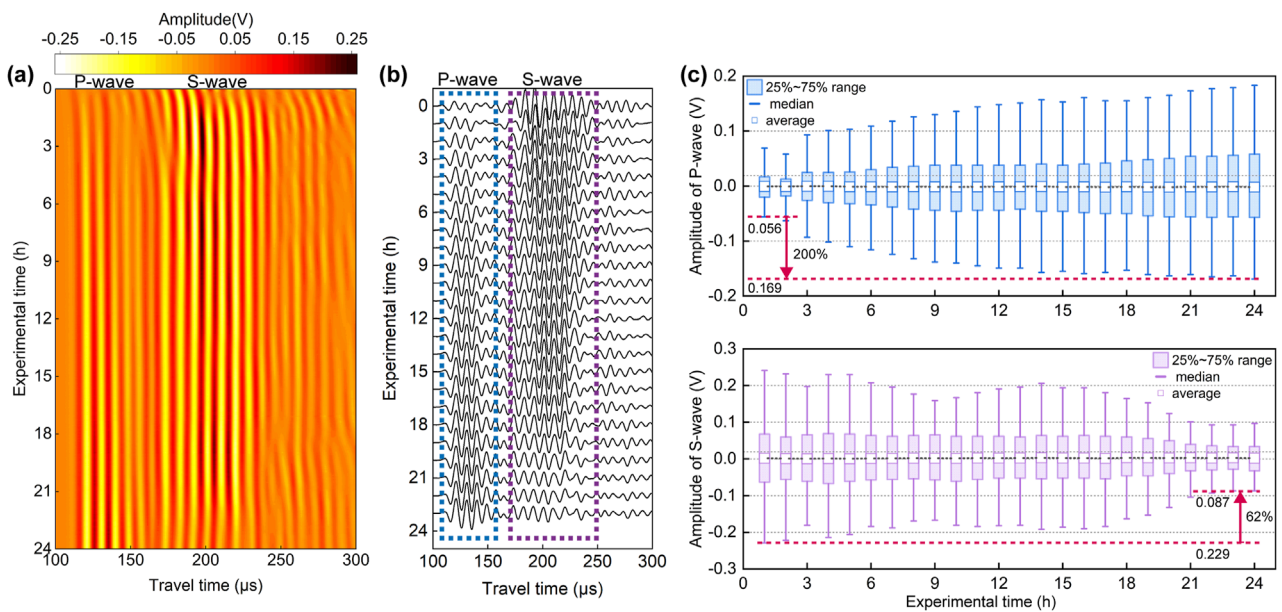


FIGURE 12 Time domain response to thermal cracking of water-bearing coal. (a) Ultrasonic logging map; (b) Ultrasonic P-wave and S-wave segmentation; (c) P-wave and S-wave amplitudes.

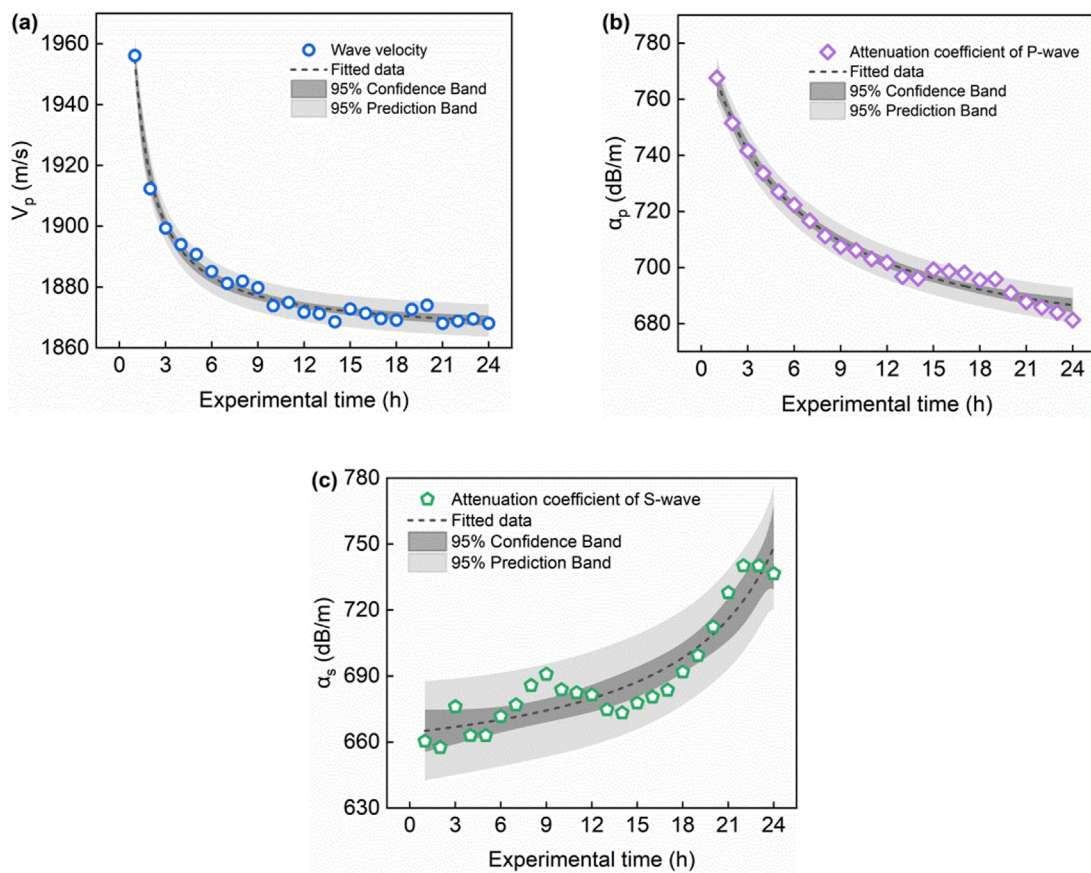


FIGURE 13 Time history of ultrasonic P-wave and S-wave characteristics during the thermal cracking process. (a) Wave velocity; (b) Attenuation coefficient of P-wave; (c) Attenuation coefficient of S-wave.

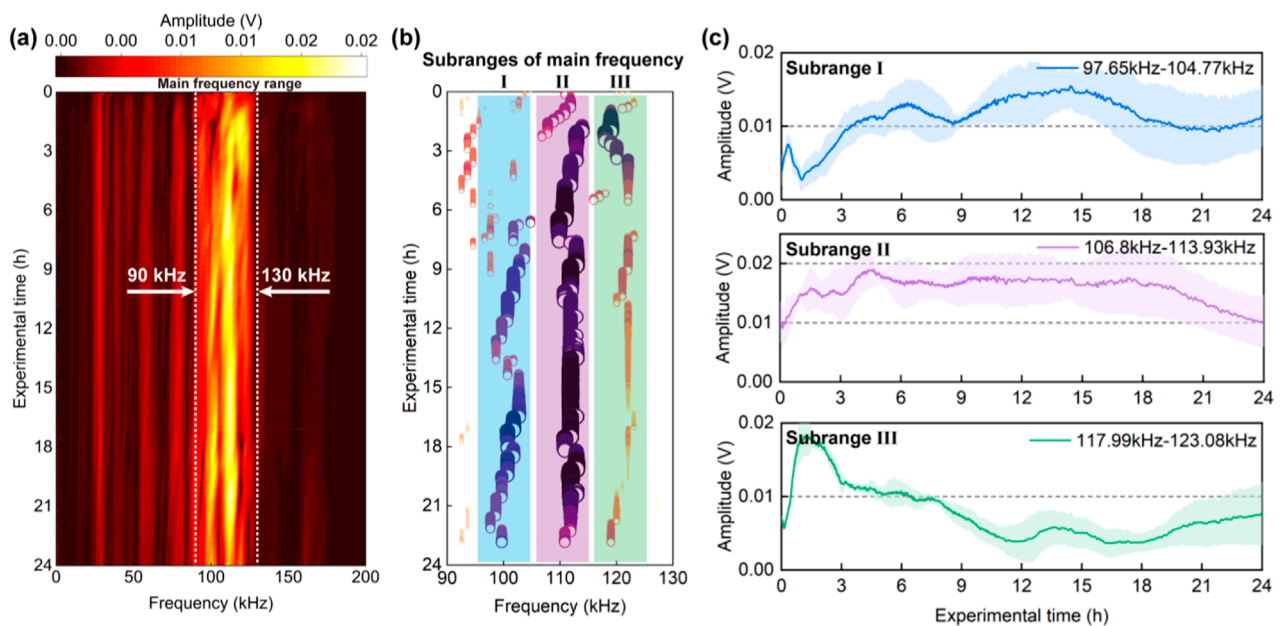
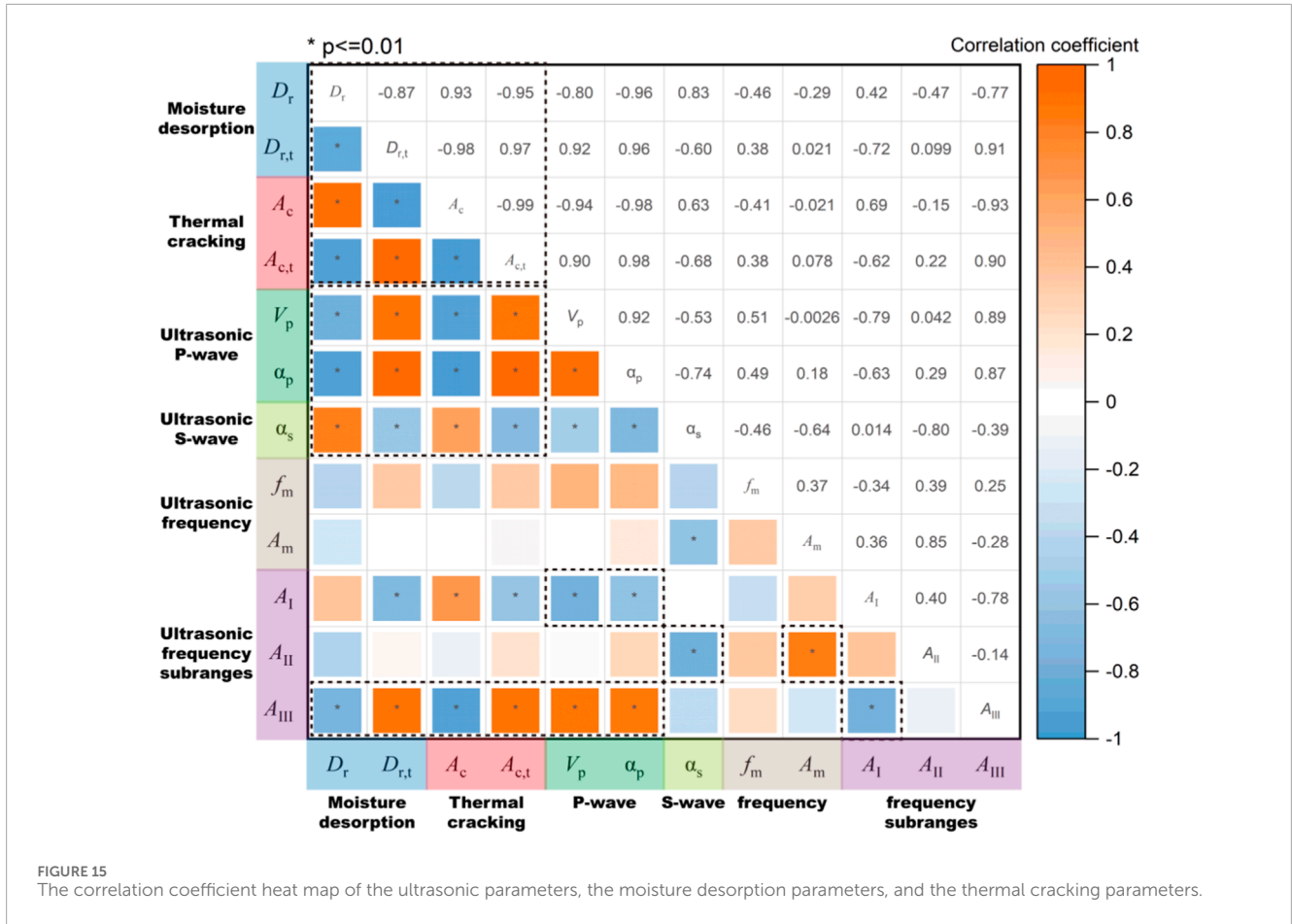


FIGURE 14 Frequency domain response to thermal cracking of water-bearing coal. (a) Spectrum logging map; (b) The frequency of subranges; (c) The amplitudes of subranges.



desorption, respectively, which are calculated by

$$D_r(t) = \frac{m_w - m_s(t)}{\rho m_w}, D_{r,t}(t) = \frac{\partial D_r(t)}{\partial t} \quad (1)$$

where $D_r(t)$ is the accumulated moisture desorption amount, $D_{r,t}(t)$ is the moisture desorption rate, $m_s(t)$ is the real-time mass of coal during the moisture desorption process, m_w is the mass of saturated coal, and ρ is the density of moisture. The cumulative moisture desorption amount and moisture desorption rate were obtained by Equation 1, and the results were illustrated in Figures 4a, b, respectively. The cumulative moisture desorption amount increased by 31.40 cm³/kg over 24 h, revealing significant nonlinear characteristics in its variation over time, as indicated by the data fitting results. This nonlinear behavior can be expressed by the power function $D_r = 3.27t^{0.71}$. Conversely, the moisture desorption rate initially decreased rapidly with time before stabilizing at a low level, exhibiting distinct stage characteristics throughout the process. Specifically, the moisture desorption rate decreased by nearly 68% during the first 6 h, followed by a gradual change of only 32% from 6 to 24 h. Consequently, the moisture desorption process was categorized into two stages: a rapid desorption stage, characterized by a significant decrease in the moisture desorption rate, and a steady desorption stage, during which the rate remained consistently low. The time history of cumulative moisture desorption amount demonstrated a nonlinear increasing trend during the rapid desorption stage, while it exhibited

an almost linear increasing trend in the steady desorption stage. In addition, It can be noted from Figure 4c that the aperture of the primary crack on the coal surface expands during the moisture desorption process, particularly within the first 6 h. During this initial period, the crack aperture increases significantly, and a new crack forms beneath the primary crack. The experimental results indicate that the coal sample undergoes rapid moisture desorption during the first 6 h, suggesting a strong correlation between this rapid desorption phase and the thermal cracking of coal.

The crack features observed during the thermal cracking process were further analyzed using image processing techniques, with the results illustrated in Figure 5. Initially, images of the primary crack, with dimensions of 1,000 pixels × 1,000 pixels, and images of the new crack, measuring 500 pixels × 500 pixels, were selected as regions of interest (ROIs). The basic contours of the cracks were obtained through sketching, as depicted in Figures 5a, d. Four sampling lines were established at equal intervals along the vertical direction within the ROI, allowing for the extraction of grey scale values along these lines to generate profile lines of the coal surface. The undulation characteristics of these profile lines facilitated the identification of the start and end points of the crack boundary, with results presented in Figures 5b, e. Utilizing the identified start and end points of the crack boundary, the crack aperture values and crack opening speeds at various locations were calculated, as shown in Figures 5c, f. The expansion phenomena were observed at different positions of the primary crack, as illustrated in Figure 5c, with the

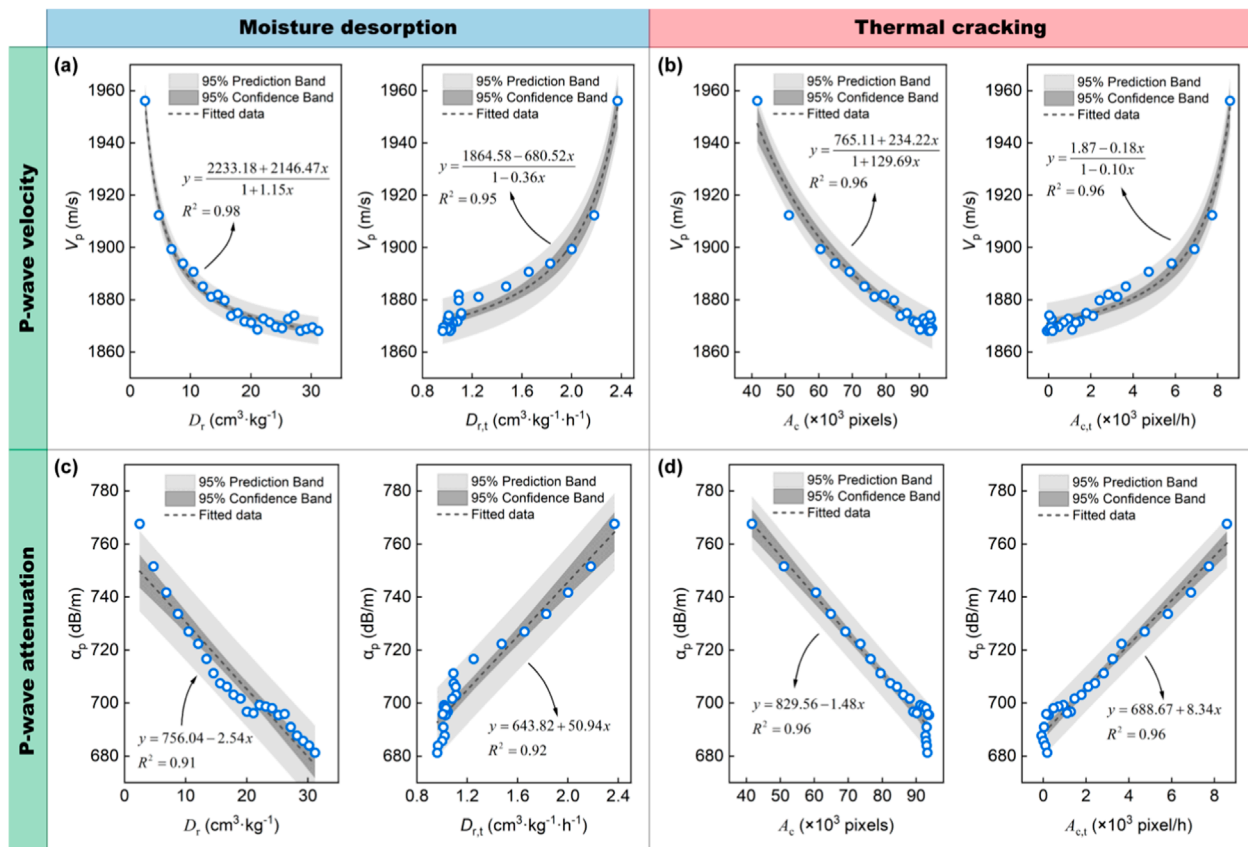


FIGURE 16

Correlation analysis of the ultrasonic parameters with moisture desorption and thermal cracking parameters of water-bearing coal.

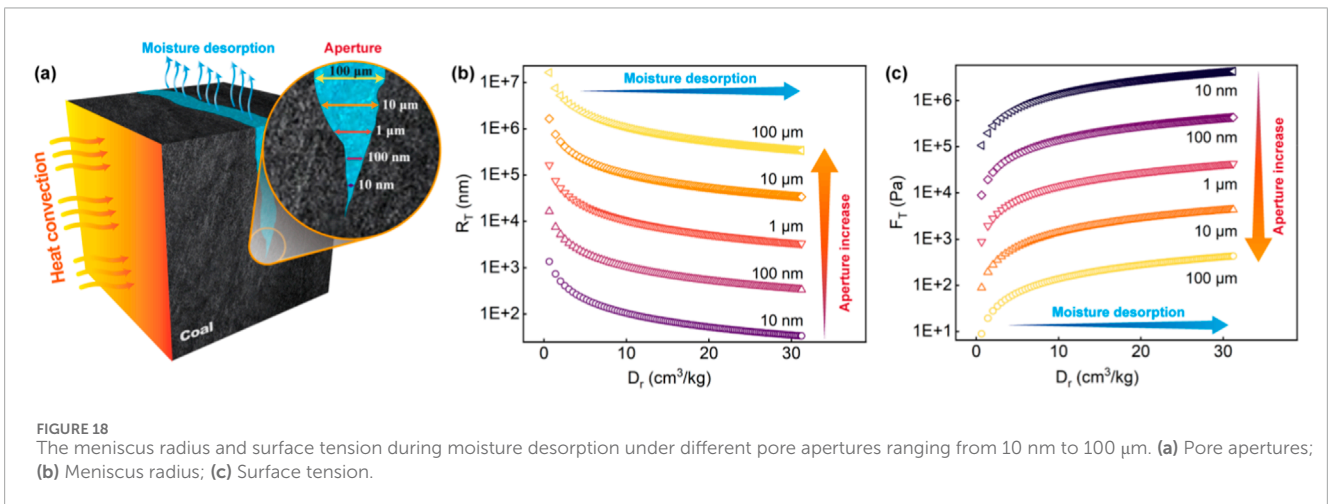
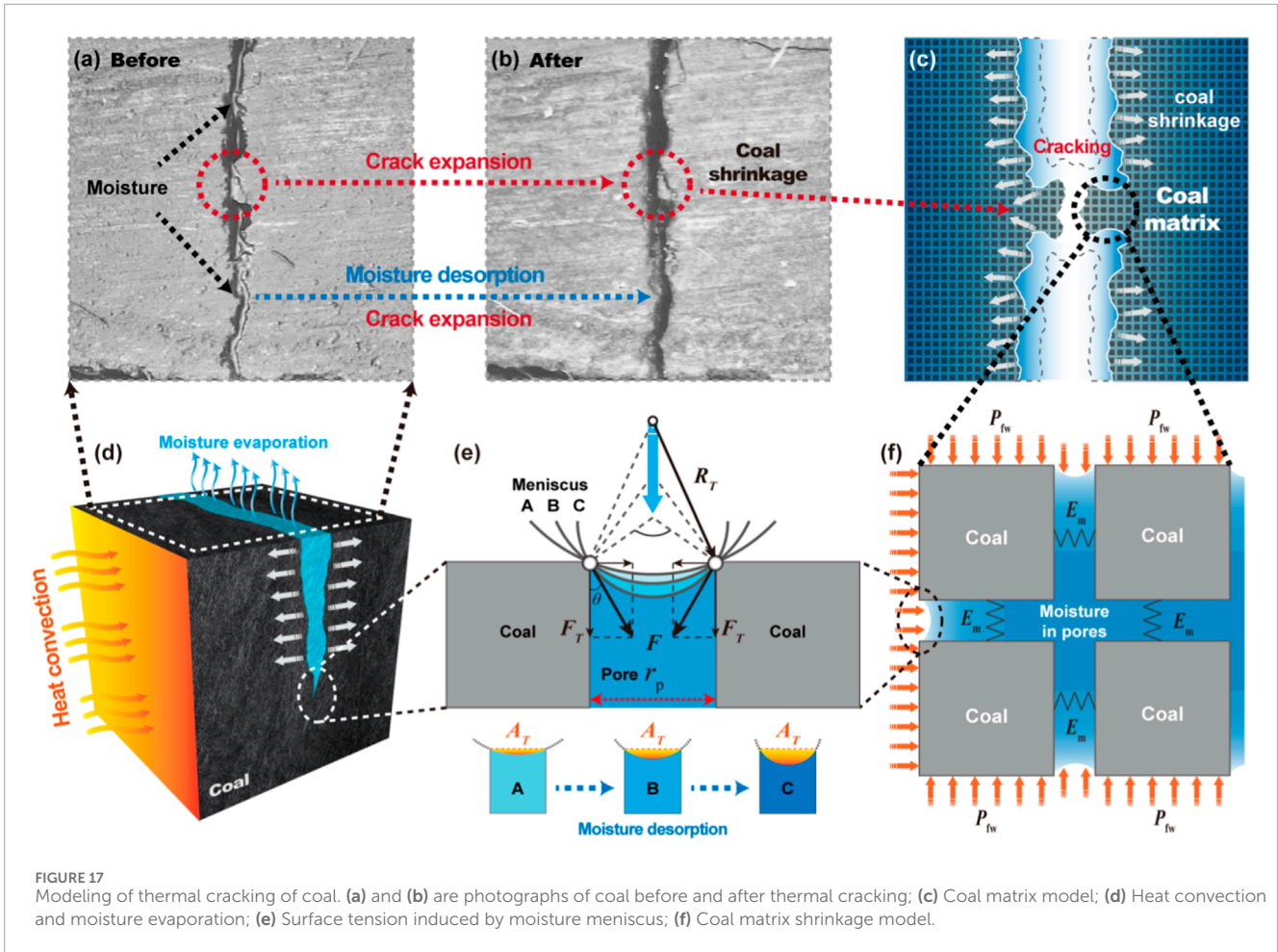
crack aperture generally exhibiting an increasing trend over time. During the thermal cracking process, the aperture at the middle positions of the primary crack (Sampling Line II and Sampling Line III) accounted for as much as 73%, while the aperture proportions at the two end positions (Sampling Line I and Sampling Line IV), although initially lower, increased rapidly throughout the thermal cracking process, ultimately becoming comparable to that of the middle positions.

In addition, the thermal cracking velocities are initially larger but decrease rapidly over time. During the initial stage of cracking, the expansion velocity at the crack tip (Sampling Line IV) predominates, exhibiting a velocity two to three times greater than that observed in the middle of the crack (Sampling Lines II and III). This observation indicates that the opening of the primary crack is primarily driven by the tip cracking, while the middle of the crack expands slowly throughout the process. Additionally, as illustrated in Figure 5f, the coal sample begins to crack after 3 h in a high-temperature environment, with the cracking opening speed reaching its peak around 9 h before rapidly declining into a slow cracking stage. Notably, the cracking opening speed at the tips accounts for as much as 59%, suggesting that new cracks primarily expand at the tips, with the middle region of the crack being driven by the expansion occurring at the tips.

To further investigate the relationship between the thermal cracking process and moisture desorption in water-bearing coal,

we extracted binary images of primary and newly formed crack morphologies using the threshold method, as illustrated in Figures 6a, d. By identifying the primary crack features in the binary map, we calculated the areas of both primary and new cracks, with the time history of the crack area and crack expansion speed presented in Figures 6b, e. The results indicate that the areas of both primary and new cracks exhibit a trend of rapid increase followed by gradual stabilization, while the crack expansion speed demonstrates a trend of rapid decrease followed by gradual stabilization. Notably, both trends over time exhibit significant nonlinear characteristics.

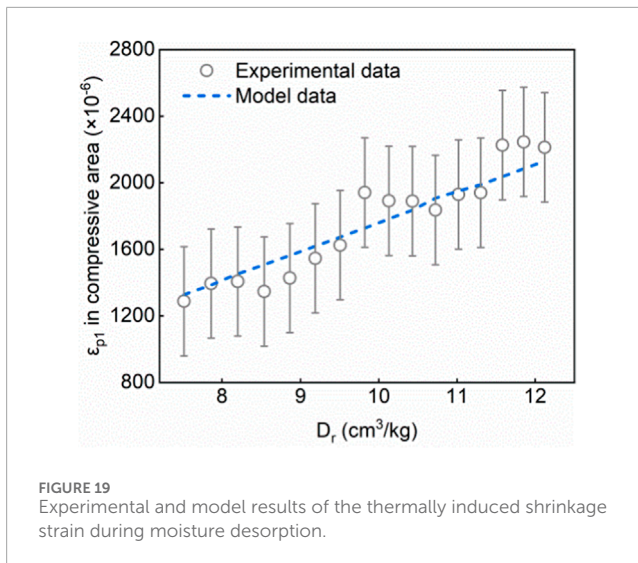
Furthermore, it can be seen from Figures 6a, d that during the thermal cracking process of water-bearing coal, the variation of the crack area is mainly caused by the change of the crack aperture (i.e., the length of the short axis of the ellipse enclosing the crack). Therefore, the crack morphology area can be used to characterize the crack aperture, and the rate of change of the crack morphology area can be used to characterize the crack expansion speed. The relationship between the thermal cracking behavior (denoted by crack aperture and crack expansion speed) and the moisture desorption properties (characterized by accumulated moisture desorption amount and moisture desorption rate) was further investigated and the results are shown in Figures 6c, f. It can be found that the variation of the crack area with the cumulative moisture desorption amount shows a rapid increase



followed by a gradual stabilization, while the crack expansion speed showed a linear increase with the moisture desorption rate. The data fitting results indicate that there is a nonlinear positive correlation between the crack aperture and the cumulative moisture desorption amount, while there is a linear positive correlation between the crack expansion speed and the moisture desorption rate.

3.2 Strain field evolution during the thermal cracking process of coal

According to rock fracture mechanics, crack initiation and expansion are closely related to the internal strain field, particularly in the tip zone of the crack, known as the fracture process zone (FPZ). Therefore, investigation of the FPZ based on the



strain field is essential for further elucidating the mechanism of thermal cracking of water-bearing coal. The commonly used FPZ monitoring techniques can be categorized into three groups (Kong, et al., 2024; Zhang and Zhou, 2022): (1) image-based methods, such as microscopy and digital image correlation (DIC); (2) acoustic-based methods, including acoustic emission (AE) and ultrasonic testing; and (3) mechanical-based methods, such as Nano-indentation. Currently, image-based methods are particularly popular due to their ease of implementation and ability to accurately capture the full-field displacement and strain, thereby enhancing the identification accuracy of the FPZ. Consequently, this study employs the microscopic image-based DIC technique to investigate the evolution of the FPZ during the thermal cracking process of water-bearing coal.

The experimental results from the thermal cracking process in water-bearing coal indicate that crack initiation and expansion predominantly occur within the initial 3–6 h. To analyze the evolution characteristics of the strain field during this critical period, this study focuses on crack images captured within the specified timeframe. For further analysis, a region of interest (ROI) of 400 pixels by 400 pixels, centered on the newly formed crack, is selected from each image, with an image resolution of 2 $\mu\text{m}/\text{pixel}$. The digital image correlation (DIC) method is employed to investigate the FPZ, specifically utilizing the maximum principal strain to delineate the boundaries of the FPZ. Consequently, this paper primarily focuses on calculating the maximum principal strain field throughout the thermal cracking process, with the results illustrated in Figure 7.

The findings reveal that within the first 30 min, a strain concentration zone gradually develops at the center of the ROI. Over time, the principal strain values within this concentration zone increase rapidly, creating a high strain gradient compared to the adjacent regions. Furthermore, an analysis of the strain orientation shows a predominant alignment of the strain field between 90° and 120°. Remarkably, this strain concentration area exhibits stable expansion in this orientation throughout the thermal cracking process, with no bifurcation phenomena observed. This stability and path dependence in the thermal cracking behavior of coal suggests that crack expansion is consistently and steadily driven

along pre-existing paths following the formation of new cracks influenced by the principal strain. This understanding of crack evolution under thermal conditions is essential for predicting coal behavior in applications such as CBM extraction.

The determination of the FPZ boundary relies on analyzing the maximum principal strain field. This method establishes that 70% of the peak maximum principal strain serves as the boundary threshold for the FPZ, as referenced in (Dutler, et al., 2018). Statistical analysis of the principal strain field, presented in Figure 8a, reveals that the average principal strain in the coal exhibits an almost linear growth trend over time, culminating in a peak value of 0.028 at $t = 170$ min. Accordingly, the threshold for the FPZ, calculated as 70% of this peak value, is approximately 0.0196. When the maximum principal strain exceeds this threshold, it indicates that the FPZ has been entered.

The FPZ results are obtained and illustrated in Figures 8b, c. A closer examination of the maximum principal strain and FPZ width uncovers that the peak maximum principal strain crosses the threshold at $t = 30$ min, marking the emergence of the FPZ at that time. Initially, the width of the FPZ is a mere 20 pixels (approximately 40 μm). As the maximum principal strain continues to increase, the width of the FPZ exhibits a rapid initial expansion, followed by a trend toward gradual stabilization, ultimately reaching 70 pixels (about 140 μm) at $t = 170$ min. By analyzing the maximum principal strain field and establishing the FPZ boundaries, we can further gain insights into the mechanisms driving crack formation and growth. The observed results emphasize the dynamic behavior of the FPZ in water-containing coals during thermal cracking, showcasing how strain influences the evolution of the FPZ over time.

To further investigate the factors contributing to the expansion of the FPZ, we examined the distribution of the maximum principal strain in the non-FPZ by excluding areas where the maximum principal strains exceed 70%, as illustrated in Figure 9a. The figure reveals a significant gradient of the maximum principal strain near the FPZ boundary, followed by a more uniform shrinkage strain (i.e., where the maximum principal strain value is negative) in the non-FPZ. Notably, the area of the shrinkage region in the non-FPZ progressively expands with an increase in FPZ width. A probability density analysis of the maximum principal strain in the non-FPZ indicates that the dominant strain gradually shifts from the tensile to the compressive region over time, with a pronounced compressive zone emerging with a high probability around $t = 170$ min, as shown in Figure 9b.

Furthermore, statistical analysis of the maximum principal strains in the non-FPZ reveals that during the interval of 0–80 min, the non-FPZ is predominantly characterized by the tensile region; however, the intensity of the tensile strain gradually diminishes, as shown in Figure 9c. After $t = 80$ min, the non-FPZ transitions to being dominated by the compressive region, with the intensity of the compressive strain steadily increasing. Additionally, the proportion of the compressive region consistently rises with FPZ expansion, surpassing 50% at $t = 80$ min, thereby providing further evidence that matrix shrinkage significantly influences the thermal cracking of coal.

The relationship between thermal cracking and matrix shrinkage of water-bearing coals was investigated, and the FPZ width and crack area were selected as indicative parameters of thermal cracking. In addition, shrinkage strain and shrinkage area

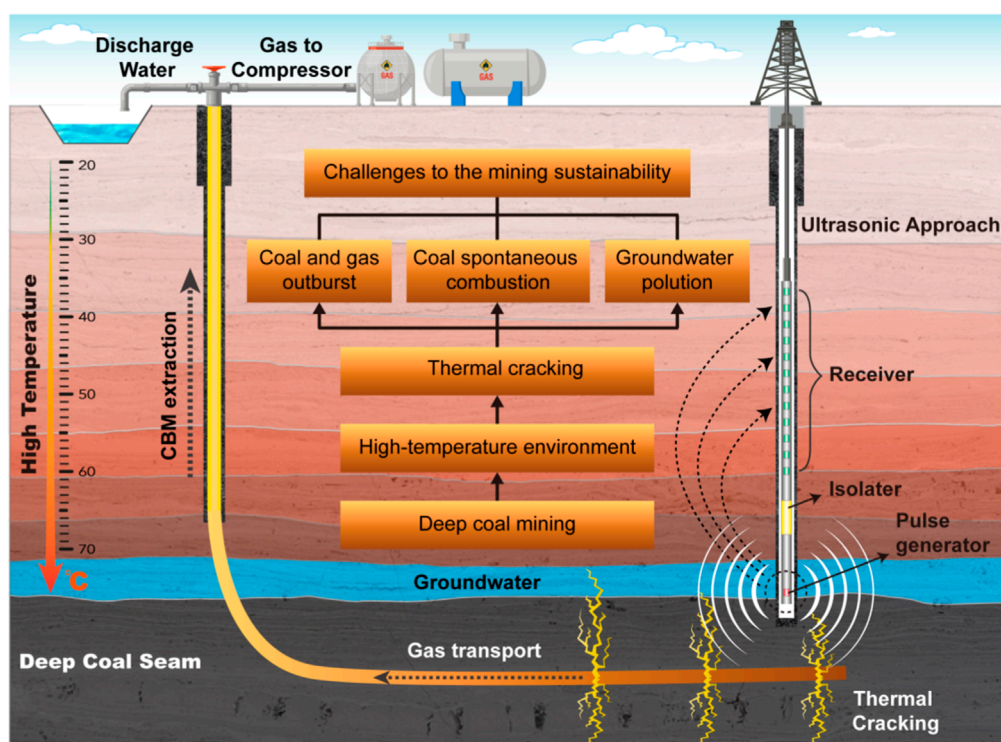


FIGURE 20 Schematic of assessing the coal thermal cracking by ultrasonic approach in deep coal mining.

were used to characterize coal shrinkage. A correlation analysis was carried out between the thermal cracking parameters and the shrinkage parameters and the results are presented in Figure 10. The figure shows that the thermal cracking parameters increase progressively as the shrinkage parameters rise, indicating a significant positive linear correlation. These findings suggest that the thermal cracking process of coal is fundamentally associated with the matrix shrinkage effect; specifically, a larger matrix shrinkage area and a higher intensity of shrinkage strain correspond to a more pronounced degree of thermal cracking in the coal. The correlation results indicate that applying heat to coal induces the penetration of thermal energy into the material, leading to an increase in internal temperature. This thermal rise facilitates the desorption of moisture from the coal matrix. As moisture is removed, the internal structure of the coal undergoes shrinkage. This shrinkage generates internal stresses within the coal matrix, which, when exceeding the material's tensile strength, results in the initiation and expansion of cracks.

3.3 Ultrasonic response to the thermal cracking process of coal

Thermal cracking of water-bearing coal in a high-temperature environment occurs not only on the surface of the coal but also within its internal structure due to heat conduction. An ultrasonic detection method was therefore required to investigate the internal thermal cracking of the coal, the results of which are shown in Figure 11. The original data of the ultrasonic waves are

available in the Supplementary Video 2. The time-domain results indicate that the ultrasonic waveform lasts approximately 200 μ s, with intensity fluctuating between -0.2 V and 0.2 V. Notably, it displays a clear demarcation between P-wave and S-wave, facilitating further differentiation between these two wave types. An analysis of the ultrasonic spectrum reveals that the primary frequency consistently diminishes throughout the thermal cracking process of the coal. Initially, a single broad-domain frequency peak is observed at $t = 1$ h, which gradually disintegrates into a narrower frequency peak by $t = 3$ h, ultimately resulting in two primary frequency peaks of comparable strength after $t = 12$ h. This indicates that the frequency spectrum of the ultrasonic wave is sensitive to the thermal cracking process.

In ultrasonic testing, P-waves and S-waves are two basic types of elastic waves. The physical responses of these two waveforms have significant differences: P-waves are sensitive to open fractures and their attenuation can characterize the opening characteristics of the fractures, while S-waves are more sensitive to closed fractures and can detect the shear-slip characteristics of the fractures. Therefore, in this study, the characteristic parameters of P-waves are used to investigate the opening patterns of thermal cracks, while the characteristic parameters of S-waves can be used to investigate the shear-slip characteristics of the fractures. Since the velocity of P-waves is greater than that of S-waves, this study distinguishes between P-waves and S-waves by analyzing the time difference between their arrivals. The P- and S-waves were extracted from the ultrasonic results, and their amplitudes were analyzed to assess the ultrasonic response to the internal thermal cracking of the

coal. As shown in Figures 12a, b, the P-wave duration ranges from approximately 110 μs –160 μs , while the S-wave duration ranges from nearly 160 μs to 260 μs . Notably, the amplitude and duration of the S-wave are greater than those of the P-wave. Furthermore, Figure 12c illustrates that the P-wave amplitude increases from 0.056 V to 0.169 V, representing an increase of up to 200%. This increase in P-wave amplitude primarily occurs within the first 6 h, exhibiting an overall trend of initially rapid growth followed by a slower increase. In contrast, the S-wave amplitude decreases over time from 0.229 V to 0.087 V, resulting in an overall reduction of approximately 62%. However, the variation in S-wave amplitude is characterized by fluctuations, initially decreasing and then increasing around $t = 9$ h, before continuing to decrease after $t = 15$ h.

To further analyze the variation in ultrasonic wave parameters during the thermal cracking process, we calculate the ultrasonic wave velocity and attenuation coefficient based on Equations 2, 3, respectively.

$$v = l / (t_2 - t_1) \quad (2)$$

$$\alpha = -[20 \log_{10}(A_2/A_1)] / l \quad (3)$$

where v is the wave velocity; α is the attenuation coefficient; t_1 is the incident time of the ultrasonic wave; t_2 is the received time of the ultrasonic wave; l is the traveling distance, i.e., the sample length; A_1 and A_2 are the amplitudes of the incident and received ultrasonic waves, respectively.

The results in Figure 13 illustrate that both the velocity and attenuation coefficient of P-waves exhibit a trend of rapid decline followed by gradual stabilization over time, indicating significant nonlinear characteristics characterized by the function $y = a/(bx + c) + d$. Conversely, the attenuation coefficient of S-waves displays a fluctuating upward trend over time, which also exhibits nonlinear features and can be fitted by the same function, achieving a fitting goodness of 0.85. These results indicate that both the ultrasonic wave velocity and the attenuation coefficient are responsive to the thermal cracking behavior of water-bearing coal, rendering them the preferred parameters for evaluating the thermal cracking process.

In addition, the frequency of ultrasonic wave propagation is closely related to the scale characteristics of fractures. The opening of these fractures significantly affects the propagation characteristics of ultrasonic waves of different frequencies. In general, high-frequency ultrasonic waves have shorter wavelengths that are comparable to or smaller than the scale of the fractures, making them susceptible to scattering, reflection, and diffraction at fracture interfaces. As a result, high-frequency components experience rapid attenuation that increases nonlinearly with increasing frequency. In contrast, low-frequency ultrasonic waves have longer wavelengths that can bypass smaller fractures, allowing them to propagate with relatively less attenuation. By analyzing the propagation patterns of ultrasonic waves in different frequency bands, we can infer the opening evolution patterns of fractures at different scales, providing valuable insights for evaluating thermal cracking in coal. In this study, the primary frequency range of the ultrasonic spectrum is between 90 kHz and 130 kHz, as shown in Figure 14a. Further examination of this range reveals three distinct subranges of dominant frequencies: 97 kHz–104 kHz, 106 kHz–113 kHz, and 117 kHz–123 kHz. Based on these clustering characteristics, we

classify the ultrasonic frequency spectrum into subranges I, II, and III, respectively, to more accurately reflect the thermal crack evolution of different patterns. Figure 14b indicates that among the three subranges, the subrange II exhibits greater stability in its peak frequency, while the peak frequencies in subranges I and III display fluctuations. The amplitude of the peak frequency in subrange III shows a continuous decline, with its amplitude significantly lower than that of subranges I and II. Statistical analysis of the amplitudes for the three subranges is presented in Figure 14c, revealing distinct evolutionary patterns in amplitude across the different frequency ranges. The amplitude of the subrange I demonstrates a generally increasing trend, with a brief drop occurring near $t = 9$ h; the subrange II maintains a more stable and elevated trend, gradually decreasing after $t = 18$ h; whereas the subrange III shows an initial slight increase followed by a continuous decrease. According to ultrasonic theory, the attenuation of ultrasonic waves across different frequency ranges correlates with the scale of internal defects within the medium. Thus, the amplitudes in these subranges can serve as characteristic parameters for assessing the evolution of cracks of varying scales.

The correlation coefficient heat map, which illustrates the relationships among the ultrasonic parameters (V_p , α_p , α_s , f_m , A_m , A_1 , A_2 , A_3), moisture desorption parameters (Dr , D_{rt}), and thermal cracking parameters (A_c , A_{ct}), was generated through correlation analysis, as depicted in Figure 15. The results indicate a strong correlation between the moisture desorption parameters and the thermal cracking parameters, with correlation coefficients exceeding 0.87. Additionally, the correlation coefficients between the ultrasonic P-wave parameters and both the moisture desorption parameters and thermal cracking parameters were all greater than 0.8. Notably, the correlation coefficients involving the P-wave attenuation coefficients, moisture desorption parameters, and thermal cracking parameters exceeded 0.95. This finding suggests that the P-wave exhibits a favorable response to the moisture desorption and thermal cracking processes, indicating that the P-wave attenuation coefficient should be prioritized when evaluating the thermal cracking behavior of coal. Furthermore, the correlation coefficients of the P-wave attenuation coefficients with the cumulative moisture desorption amount and thermal cracking area were positive, while those for the S-wave were negative. This indicates that the moisture desorption and thermal cracking processes enhance P-wave propagation while diminishing S-wave propagation.

In contrast, the correlation coefficients between the peaks across the full frequency range and the parameters of moisture desorption and thermal cracking were low (<0.8) with the S-wave parameters, while the amplitude of subrange III demonstrated a strong correlation (>0.87) with the P-wave parameters. This indicates that subrange II corresponds to the S-wave of the ultrasonic wave, and subrange III corresponds to the P-wave. Furthermore, the correlation coefficient between the amplitude of subrange III and the moisture desorption and thermal cracking parameters was also high (>0.87), suggesting that subrange III can effectively be employed to assess the moisture desorption and thermal cracking of coal.

Based on the results of the correlation analysis, a regression fitting was performed on the P-wave parameters, moisture desorption parameters, and thermal cracking parameters, with the results illustrated in Figure 16. The figure indicates that the P-wave

velocity exhibits a nonlinear relationship with both the moisture desorption and thermal cracking parameters, conforming to the functional model $y = (a+bx)/(1+cx)$. Here, parameters a , b , and c represent the model fitting coefficients, with a goodness-of-fit exceeding 0.95. The fitting results reveal that the P-wave velocity demonstrates a nonlinear decreasing trend as the cumulative moisture desorption amount and crack area increase, while it shows a nonlinear increasing trend with the rise in moisture desorption rate and crack expansion rate.

Additionally, the P-wave attenuation coefficient exhibits a linear decreasing trend with increasing cumulative moisture desorption and crack area, while showing a linear increasing trend with rising moisture desorption rate and crack expansion rate. The linear relationship between the P-wave attenuation coefficient, moisture desorption parameters, and thermal cracking parameters conform to the functional model $y = a + bx$, where parameters a and b represent the model fitting coefficients, and the goodness-of-fit exceeds 0.90. Overall, the ultrasonic P-wave parameters demonstrate a strong response to the moisture desorption and thermal cracking parameters, thus serving as effective indicators for assessing the degree of moisture desorption and thermal cracking in coal subjected to high-temperature conditions.

4 Discussion

4.1 Mechanism and modeling of the thermal cracking process of coal

Coal is a porous medium characterized by a complex pore and fissure structure. These pores and fissures serve as the storage space and migration channel for moisture, playing a critical role in regulating moisture desorption within coal. Free moisture is found in macro fissures and pores, allowing for easy movement and evaporation (Feng et al., 2018). Capillary moisture resides in micropores, maintaining stability through capillary action (Zhang et al., 2019). Adsorbed moisture is tightly bound to surface micropores and fissures through van der Waals forces or hydrogen bonding, making evaporation challenging (Nwaka et al., 2016). When coal is exposed to a high-temperature environment, the moisture within its pores and cracks begins to desorb. Initially, the free water, which is associated with the macroscopic cracks, undergoes a desorption process akin to direct evaporation due to the absence of capillary forces. When the free water is exhausted, the liquid water within the coal cannot sustain a continuous flow. A portion of the liquid water is adsorbed onto the surface of the coal matrix due to capillary forces, while another portion exists in a saddle-like configuration within the coal pores. As the moisture continues to diminish, some of the moisture undergoes a phase transition from liquid to gas, migrating to the surface of the coal through the cracks, driven by internal diffusion processes. Simultaneously, another fraction of the moisture transitions from the capillaries into the crack spaces, influenced by external factors such as heat and airflow. The presence of evaporated water can elevate the internal pressure within the coal, creating a pressure gradient that facilitates the migration of moisture toward the coal surface. Then the moisture mixes with the flowing air and is ultimately expelled from the coal matrix. It can be concluded that as

moisture desorption progresses, the evaporation of moisture from the coal begins to affect the micro-cracks and pores. This desorption results in a reduction in pore pressure, leading to a gradual collapse of the pore structure and the formation of new microscopic cracks. Furthermore, as the moisture continues to desorb, the density of the micro-cracks increases and they converge to form larger cracks, which are referred to as macroscopic thermal cracking.

To quantitatively describe the mechanism of thermal cracking in coal, we derived an equation relating the driving force of thermal cracking to the moisture desorption of the coal. A thermal cracking model of the coal was established as shown in Figure 17. This model simplifies the coal structure to a combination of matrix and cracks, where the cracks separate the matrix components and are filled with moisture. As the moisture gradually evaporates in the high-temperature environment, the surface tension and vapor pressure act on the crack surface initiating the thermal cracking phenomenon. Typical photographs illustrating the phenomenon before and after thermal cracking are shown in Figures 17a, b. The experimental results of the strain field at the tip of the thermal crack indicate that thermal cracking is a typical type of tensile fracture. Throughout the cracking process, the coal matrix on both sides of the crack experiences shrinkage deformation, as depicted in Figure 17c.

Firstly, surface tension, one of the main driving forces of thermal cracking, is intrinsically related to the moisture in the cracks. As this moisture gradually evaporates due to thermal effects, it forms a curved surface, i.e., a water meniscus, which generates surface tension along the tangent direction at the contact point, as shown in Figures 17d, e. The expression for this surface tension is:

$$F = \pi \gamma r_p \quad (4)$$

where F is the surface tension of moisture, γ is the surface energy of moisture, and r_p is the aperture of the micro-crack and pore. It can be seen from Figure 17e that the effect of surface tension on the crack expansion is mainly caused by the component F_T perpendicular to the crack surface, and the relationship between them is $F_T = F \cos(\theta)$. θ is the contact angle, and the relationship between the contact angle, pore aperture, and the radius of the moisture meniscus is $\cos(\theta) = r_p/2R_T$, and substituting into Equation 4, it can be obtained that the stress component of surface tension, F_T , is

$$F_T = \frac{4\pi \gamma r_p \cos(\theta)}{\pi r_p^2} = \frac{2\gamma}{R_T} \quad (5)$$

where R_T is the radius of the moisture meniscus. Since the moisture surface energy γ remains constant at a given temperature, it can be deduced from Equation 5 that the stress component F_T and the radius of the moisture meniscus R_T are inversely proportional. Specifically, as the radius of the moisture meniscus decreases, the surface tension increases, thereby enhancing the effect on crack expansion.

The radius of the moisture meniscus changes continuously throughout the moisture desorption process, as shown in Figure 17e. To quantitatively characterize the relationship between the radius of the moisture meniscus and moisture desorption, the coal matrix is simplified to a rectangular shape with the pores between the matrix filled with moisture. As moisture desorption occurs, the moisture content within the pores decreases, leading to a gradual reduction in the radius of the moisture meniscus. The relationship can be expressed by the non-linear Equation 6, which relates the amount

of moisture desorption to the radius of the moisture meniscus.

$$A_T = R_T^2 \arcsin\left(\frac{r_p}{2R_T}\right) - \frac{r_p \sqrt{4R_T^2 - r_p^2}}{4} = \frac{D_r \pi r_p^2}{4V_p} \quad (6)$$

where A_T is the moisture area, D_r is the moisture desorption amount, and V_p is the pore volume which can be determined by the mercury intrusion method. By substituting the experimental results of moisture desorption amount into the non-linear Equation 6, we can solve for the radius of the moisture meniscus and the resulting surface tension generated by the moisture meniscus based on Equation 5.

The results of the pore apertures, the moisture meniscus radius, and the surface tension during the moisture desorption process are shown in Figure 18. It can be seen that the radius of the moisture meniscus gradually decreases with moisture desorption, while the surface tension gradually increases. Both trends follow a significant two-step pattern: an initial rapid change followed by a slower change. In addition, for the same amount of moisture desorption, the radius of the moisture meniscus increases as the pore aperture increases, resulting in a decrease in surface tension. In addition, the results also indicate that as thermal cracking progresses, the expansion of the cracks leads to a decrease in surface tension, thereby reducing the influence of moisture. Consequently, the rate of thermal cracking in the coal may gradually slow down or even stagnate, which has been demonstrated in Figure 6 that the area of thermal cracks initially increases rapidly and then gradually stabilizes.

On the other hand, vapor pressure is another significant driving force for thermal cracking, as it is related to the vapor generated from liquid water within the coal under high thermal conditions. The vapor pressure exerted on the crack surface promotes crack expansion considerably. According to physical theory, the quantity of vapor and the surface area do not influence vapor pressure; therefore, it can be assumed that the vapor pressure is solely influenced by temperature. The relationship between vapor pressure and temperature can be described by the Clausius-Clapeyron equation, as follows:

$$\log\left(\frac{P_{fw}}{P_{fw25}}\right) = -\frac{H_{vap}}{R} \left(\frac{1}{T} - \frac{1}{T_{25}}\right) \quad (7)$$

where, P_{fw} is the vapor pressure, P_{fw25} is the vapor pressure at the standard condition (25 °C, 3.17 kPa), H_{vap} is the vaporization enthalpy of water, R is the molar gas constant, T is the temperature of the coal, and T_{25} is the thermodynamic temperature of the standard condition. Finally, the driving force of coal thermal cracking during moisture desorption can be obtained by combining Equations 5–7, i.e.,

$$F_C = F_T + P_{fw} = \frac{2\gamma}{R_T} + P_{fw25} e^{-\frac{H_{vap}}{R} \left(\frac{1}{T} - \frac{1}{T_{25}}\right)} \quad (8)$$

Finally, the proposed model needs to be validated with experimental results. Since the surface tension and vapor pressure of moisture in the pores are difficult to measure directly, we propose an indirect method of verifying the driving forces behind thermal cracking using shrinkage strain. This is because both surface tension and vapor pressure contribute to crack expansion while also inducing matrix shrinkage strain. The strain data can be obtained using Digital Image Correlation (DIC) analysis as shown in Figure 8. The thermally induced shrinkage strain during moisture desorption

was used to calibrate the theoretical model in Equation 8. As the shrinkage strain during thermal cracking is relatively small (<0.01), it satisfies the small deformation assumption in elastic mechanics. Therefore, the relationship between shrinkage stress (the driving force) and shrinkage strain can be expressed as follows:

$$F_C \delta_{ij} = E_m \varepsilon_{ij} \quad (9)$$

where ε_{ij} is the shrinkage strain of the coal, δ_{ij} is the Kronecker delta, and E_m is the Young's modulus of coal, which has been measured in the laboratory to be 1.2 GPa. By substituting the experimental data for moisture desorption and shrinkage strain into Equation 9, the final comparison of the experimental data and model results is presented in Figure 19. The results show that the shrinkage strain of the coal gradually increases during moisture desorption, demonstrating that moisture desorption promotes the shrinkage of the coal matrix. Furthermore, the model results are in good agreement with the experimental results, confirming that the model effectively represents the mechanical mechanisms underlying the thermal cracking of coal during moisture desorption.

4.2 Ultrasonic approach for assessing thermal cracking in deep coal mining

Thermal cracking of coal in high-temperature environments poses a significant challenge to deep coal mining. This phenomenon leads to many problems, including increased risks of coal and gas outbursts, increased spontaneous combustion of coal, and groundwater pollution, which severely limit the environmental sustainability of deep coal mining. To address the challenges posed by high-temperature thermal cracking, this study proposes a method for assessing coal thermal cracking using ultrasonic technology. Ultrasonic technology offers advantages such as non-destructive testing, rapid detection, and high accuracy, enabling real-time monitoring of changes in the internal structure of coal. By analyzing the variations in ultrasonic wave velocity and attenuation coefficients, the degree of thermal cracking and the direction of crack propagation can be accurately assessed.

The schematic of assessing thermal cracking by ultrasonic approach in deep coal mining is shown in Figure 20. The results of this study indicate that the ultrasonic propagation characteristics respond well to the thermal cracking process of coal. This implies that the use of ultrasonic propagation to assess the effects of thermal cracking in deep coal seams is a promising technique, as this technique works on the principle of using a pulse generator positioned in the wellbore to emit acoustic waves into the surrounding area. These waves are then reflected by formations such as cracks, pores, and faults, allowing stratigraphic defects to be imaged. The thermal cracking results in the formation of new cracks and an increase in the aperture of existing cracks, which in turn results in a decrease in the wave velocity of the coal. The distribution and aperture of thermally induced cracks can be effectively monitored by comparing the changes in wave velocity before and after thermal cracking changes the coal seam. When the effect of thermal cracking is inadequate - characterized by a limited number of new cracks or small crack apertures - the wave velocity logging map shows minimal

changes compared to its state before thermal cracking. In contrast, if thermal cracking is significant, there would be a significant increase in both the number of new cracks and their apertures within the coal seam, leading to noticeable changes in the wave velocity logging map. Therefore, by comparing the wave velocity logging maps before and after thermal cracking, one can evaluate the degree and extent of thermal cracking effects in deep coal seams.

In addition, ultrasonic monitoring of coal thermal cracking can provide real-time data to help control disasters such as gas outbursts and spontaneous coal combustion. By continuously monitoring changes in internal cracks within the coal seam, proactive measures can be taken to prevent such disasters. In addition, ultrasonic technology can be combined with other monitoring methods to form a comprehensive disaster warning system. For example, by integrating ultrasonic monitoring data with gas concentration monitoring and geostress monitoring data, a more thorough assessment of disaster risks in deep mining environments can be achieved. This integrated monitoring approach not only improves the accuracy of disaster warnings but also provides a basis for developing scientifically sound mining plans. The use of ultrasonic technology also helps to reduce the environmental impact of coal mining. By continuously monitoring the thermal cracking characteristics of coal, coalbed methane (CBM) extraction plans can be optimized to reduce gas emissions, thereby reducing greenhouse gas emissions. Furthermore, ultrasonic technology can provide technical support for groundwater protection and surface ecological restoration, thereby mitigating the ecological damage caused by coal mining. Therefore, the ultrasonic approach is not only a promising way to evaluate the coal thermal cracking process but also an important technical support for achieving sustainable coal mining in deep, high-temperature environments.

5 Conclusion

- (1) The cumulative moisture desorption of coal in high-temperature environments exhibits a non-linear increase over time, characterized by two stages: rapid desorption and steady desorption. Data fitting indicates a non-linear correlation between cumulative moisture desorption and thermal crack aperture, while the moisture desorption rate shows a linear relationship with thermal cracking speed.
- (2) Thermal cracking of coal involves the expansion of existing cracks and the formation of new cracks. As moisture desorption increases, the crack area expands rapidly before stabilizing, with a linear relationship between crack area change and moisture desorption rate. Thermal cracking correlates with matrix shrinkage at the crack tip, showing a linear relationship with shrinkage strain and shrinkage area.
- (3) High correlations (>0.8) were observed between ultrasonic P-wave parameters (V_p , α_p) and moisture desorption (D_r , $D_{r,t}$), as well as thermal cracking parameters (A_c , $A_{c,t}$), indicating the effectiveness of ultrasonic P-waves in responding to these processes. The proposed non-linear model based on wave velocity and linear model based on attenuation

coefficient effectively evaluates coal thermal cracking behavior. Additionally, the established thermal cracking model clarifies the relationship between thermal cracking forces and moisture desorption, supporting ultrasonic assessment methods for sustainable deep mining.

Data availability statement

The original contributions presented in the study are included in the article/[Supplementary Material](#), further inquiries can be directed to the corresponding author.

Author contributions

JF: Conceptualization, Funding acquisition, Methodology, Writing – original draft, Writing – review and editing. SL: Conceptualization, Investigation, Writing – original draft. CX: Supervision, Writing – review and editing. JP: Formal Analysis, Resources, Writing – review and editing. QH: Methodology, Visualization, Writing – review and editing.

Funding

The author(s) declare that financial support was received for the research and/or publication of this article. This work was funded by the National Natural Science Foundation of China (52104175) and the China Postdoctoral Science Foundation (No. 2022M712935).

Conflict of interest

Authors JF, CX, JP, and QH were employed by Sinosteel Maanshan General Institute of Mining Research Co., Ltd.

The remaining authors declare that the research was conducted in the absence of any commercial or financial relationships that could be construed as a potential conflict of interest.

Generative AI statement

The author(s) declare that no Generative AI was used in the creation of this manuscript.

Publisher's note

All claims expressed in this article are solely those of the authors and do not necessarily represent those of their affiliated organizations, or those of the publisher, the editors and the reviewers. Any product that may be evaluated in this article, or claim that may be made by its manufacturer, is not guaranteed or endorsed by the publisher.

Supplementary material

The Supplementary Material for this article can be found online at: <https://www.frontiersin.org/articles/10.3389/feart.2025.1609410/full#supplementary-material>

Supplementary Video 1 |

Thermal cracking of coal in high temperature environment.mp4.

Supplementary Video 2 |

Ultrasonic response to thermal cracking of coal.mp4.

References

- Akbarzadeh, H., and Chalaturnyk, R. J. (2014). Structural changes in coal at elevated temperature pertinent to underground coal gasification: a review. *Int. J. Coal Geol.* 131, 126–146. doi:10.1016/j.coal.2014.06.009
- Cai, W., Dou, L., Cao, A., Gong, S., and Li, Z. (2014). Application of seismic velocity tomography in underground coal mines: a case study of yima mining area, Henan, China. *J. Appl. Geophys.* 109, 140–149. doi:10.1016/j.jappgeo.2014.07.021
- Carras, J. N., Day, S. J., Saghafi, A., and Williams, D. J. (2009). Greenhouse gas emissions from low-temperature oxidation and spontaneous combustion at open-cut coal mines in Australia. *Int. J. Coal Geol.* 78 (2), 161–168. doi:10.1016/j.coal.2008.12.001
- Dutler, N., Nejati, M., Valley, B., Amann, F., and Molinari, G. (2018). On the link between fracture toughness, tensile strength, and fracture process zone in anisotropic rocks. *Eng. Fract. Mech.* 201, 56–79. doi:10.1016/j.engfracmech.2018.08.017
- Feng, L., Yuan, C., Mao, L., Yan, C., Jiang, X., Liu, J., et al. (2018). Water occurrence in lignite and its interaction with coal structure. *Fuel* 219, 288–295.
- Feng, J., Xu, C., Yu, F., Peng, J., Huang, Q., and Jin, P. (2024). Multifractal characterization of the inhomogeneous strain evolution of the dehydrated coal: insight from coal microstructure. *Fractals-Complex Geometry Patterns Scaling Nat. Soc.* 32 (02), 2450036. doi:10.1142/s0218348x24500361
- Guo, C., Qin, Y., Ma, D., Yang, Z., and Lu, L. (2020). Prediction of geotemperatures in coal-bearing strata and implications for coal bed methane accumulation in the bide-santang basin, western Guizhou, China. *Int. J. Min. Sci. Technol.* 30 (2), 235–242. doi:10.1016/j.ijmst.2018.07.008
- Hamada, N., Koga, H., Katsuya, K., Ishida, K., Ito, H., and Kawagoshi, Y. (2024). Insight into groundwater quality change before and after the 2016 Kumamoto earthquake. *Sci. Total Environ.* 957, 177783. doi:10.1016/j.scitotenv.2024.177783
- Huang, Y., Kong, Y., Cheng, Y., Zhu, C., Zhang, J., and Wang, J. (2023). Evaluating the long-term sustainability of geothermal energy utilization from deep coal mines. *Geothermics* 107, 102584. doi:10.1016/j.geothermics.2022.102584
- Jiang, C., Wang, Y., Duan, M., Guo, X., Chen, Y., and Yang, Y. (2021). Experimental study on the evolution of pore-fracture structures and mechanism of permeability enhancement in coal under cyclic thermal shock. *Fuel* 304, 121455. doi:10.1016/j.fuel.2021.121455
- Kahraman, S., and Yeken, T. (2008). Determination of physical properties of carbonate rocks from p-wave velocity. *Bull. Eng. Geol. Environ.* 67 (2), 277–281. doi:10.1007/s10064-008-0139-0
- Kong, X., Zhan, M., Lin, H., Cai, Y., Ji, P., He, D., et al. (2024). Time-varying characteristics of acoustic emission and fractals based on information dimension during structural failure of coal subjected to uniaxial compression. *Measurement* 236, 115088. doi:10.1016/j.measurement.2024.115088
- Leucci, G., and De Giorgi, L. (2006). Experimental studies on the effects of fracture on the p and s wave velocity propagation in sedimentary rock ("calcarene del salento"). *Eng. Geol.* 84 (3), 130–142. doi:10.1016/j.enggeo.2005.12.004
- Li, H., Shi, S., Lin, B., Lu, J., Ye, Q., Lu, Y., et al. (2019). Effects of microwave-assisted pyrolysis on the microstructure of bituminous coals. *Energy* 187, 115986. doi:10.1016/j.energy.2019.115986
- Li, S., He, D., Kong, X., Lin, H., Ma, Y., Li, X., et al. (2024). Relationship between micro-pores fractal characteristics about nmr t2 spectra and macro cracks fractal laws based on box dimension method of coal under impact load from energy dissipation theory. *Chaos, Solit. and Fractals* 189, 115685. doi:10.1016/j.chaos.2024.115685
- Li, S., Tang, D., Pan, Z., Xu, H., Tao, S., Liu, Y., et al. (2018). Geological conditions of deep coalbed methane in the eastern margin of the Ordos basin, China: implications for coalbed methane development. *J. Nat. Gas Sci. Eng.* 53, 394–402. doi:10.1016/j.jngse.2018.03.016
- Lin, B., Cao, X., Liu, T., Ni, Z., and Wang, Z. (2021). Experimental research on water migration-damage characteristics of lignite under microwave heating. *Energy and Fuels* 35 (2), 1058–1069. doi:10.1021/acs.energyfuels.0c02416
- Liu, S., Wang, D., Yin, G., Li, M., and Li, X. (2020). Experimental study on the microstructure evolution laws in coal seam affected by temperature impact. *Rock Mech. Rock Eng.* 53 (3), 1359–1374. doi:10.1007/s00603-019-01978-3
- Lv, A., Aghighi, M. A., Masoumi, H., and Roshan, H. (2022). The effects of sorbing and non-sorbing gases on ultrasonic wave propagation in fractured coal. *Int. J. Coal Geol.* 249, 103906. doi:10.1016/j.coal.2021.103906
- Nwaka, D., Tahmasebi, A., Tian, L., and Yu, J. (2016). The effects of pore structure on the behavior of water in lignite coal and activated carbon. *J. Colloid Interface Sci.* 477, 138–147.
- Pashin, J. C., and McIntyre, M. R. (2003). Temperature-pressure conditions in coalbed methane reservoirs of the black warrior basin: implications for carbon sequestration and enhanced coalbed methane recovery. *Int. J. Coal Geol.* 54 (3–4), 167–183. doi:10.1016/s0166-5162(03)00034-x
- Salmachi, A., Zeinijahromi, A., Parker, H. M., Abdullhusein, A., Badalyan, A., Kwong, P., et al. (2024). Experimental investigation of alterations in coal fracture network induced by thermal treatment: implications for CO₂ geo-sequestration. *Energy* 308, 132893. doi:10.1016/j.energy.2024.132893
- Soete, J., Kleipool, L. M., Claes, H., Claes, S., Hamaekers, H., Kele, S., et al. (2015). Acoustic properties in travertines and their relation to porosity and pore types. *Mar. Petroleum Geol.* 59, 320–335. doi:10.1016/j.marpetgeo.2014.09.004
- Sun, L., Zhang, C., Cheng, W., Shi, Q., and Huang, Q. (2022). Effect of high-temperature environment of mine goaf on pore and fracture of coal. *Fuel* 325, 124810. doi:10.1016/j.fuel.2022.124810
- Teng, T., Wang, J. G., Gao, F., Ju, Y., and Jiang, C. (2016). A thermally sensitive permeability model for coal-gas interactions including thermal fracturing and volatilization. *J. Nat. Gas Sci. Eng.* 32, 319–333. doi:10.1016/j.jngse.2016.04.034
- Wei, J., Di, B., and Ding, P. (2013). Effect of crack aperture on p-wave velocity and dispersion. *Appl. Geophys.* 10 (2), 125–133. doi:10.1007/s11770-013-0379-z
- Xiao, W., Zhang, D., Li, S., and Wu, M. (2024). Microstructural and thermal properties of coal measure sandstone subjected to high temperatures. *J. Rock Mech. Geotechnical Eng.* 16 (8), 2909–2921. doi:10.1016/j.jrmge.2023.11.007
- Yang, D., Peng, K., Zheng, Y., Chen, Y., Zheng, J., Wang, M., et al. (2023). Study on the characteristics of coal and gas outburst hazard under the influence of high formation temperature in deep mines. *Energy* 268, 126645. doi:10.1016/j.energy.2023.126645
- Yang, Y., Zheng, K., Li, Z., Li, Z., Si, L., Hou, S., et al. (2019). Experimental study on pore-fracture evolution law in the thermal damage process of coal. *Int. J. Rock Mech. Min. Sci.* 116, 13–24. doi:10.1016/j.ijrmms.2019.03.004
- Yu, Y., Liang, W., Hu, Y., and Meng, Q. (2012). Study of micro-pores development in lean coal with temperature. *Int. J. Rock Mech. Min. Sci.* 51, 91–96. doi:10.1016/j.ijrmms.2012.01.010
- Zhang, J., and Zhou, X. (2022). Fracture process zone (fpz) in quasi-brittle materials: review and new insights from flawed granite subjected to uniaxial stress. *Eng. Fract. Mech.* 274, 108795. doi:10.1016/j.engfracmech.2022.108795
- Zhang, Z., Wang, E., Liu, X., Zhang, Y., Li, S., Khan, M., et al. (2021). Anisotropic characteristics of ultrasonic transmission velocities and stress inversion during uniaxial compression process. *J. Appl. Geophys.* 186, 104274. doi:10.1016/j.jappgeo.2021.104274
- Zhang, X., Zhang, C., Feng, X., Yu, S., Li, X., Fang, Q., and Chen, G. (2019). Study on the moisture adsorption isotherms and different forms of water for lignite after hydrothermal and thermal upgrading. *Fuel* 246, 340–348.

Glossary

D_T	Accumulated moisture desorption amount (cm^3/kg)
$D_{r,t}$	Moisture desorption rate ($\text{cm}^3 \cdot \text{kg}^{-1} \cdot \text{h}^{-1}$)
m_w	Mass of the saturated coal (kg)
ρ	Density of the moisture (kg/m^3)
γ	Surface energy of moisture (J/m^2)
θ	Contact angle of moisture ($^\circ$)
F	Surface tension of moisture (N)
A_T	Moisture area (m^2)
A_c	Crack area (pixel)
$A_{c,t}$	Crack expansion speed (pixel/h)
ϵ_{p1}	Maximum principal strain
W_{FPZ}	Width of the fracture process zone (pixel)
$A_{\text{non-FPZ}}$	Area of the non-fracture process zone (pixel)
v	Ultrasonic wave velocity (m/s)
l	Travel distance of ultrasonic wave (mm)
f_m	Main frequency of the ultrasonic wave (kHz)
A_m	Amplitude of the main frequency wave (V)
α_p, α_s	Attenuation coefficient of the ultrasonic P-wave and S-wave (dB/m)
t_1, t_2	Time of the incident and received ultrasonic waves (s)
A_1, A_2	Amplitude of the incident and received ultrasonic waves (V)
A_I, A_{II}, A_{III}	Amplitude of the ultrasonic subranges I, II, and III (V)
r_p	Aperture of the micro-crack and pore (nm)
R_T	Radius of the moisture meniscus (nm)
F_T	Surface tension component contributes to the crack expansion (N)
V_p	Pore volume of coal (m^3/kg)
P_{f_w}	Vapor pressure of moisture (Pa)
P_{f_w25}	Vapor pressure at the standard condition (Pa)
H_{vap}	Vaporization enthalpy of water (J/mol)
R	Molar gas constant ($8.314 \text{ J} \cdot \text{mol}^{-1} \cdot \text{K}^{-1}$)
T	Temperature of the coal (K)
E_m	Young's modulus of coal (GPa)
ϵ_{ij}	Shrinkage strain of the coal
δ_{ij}	Kronecker delta